

A mechanistic model to assess the effectiveness of test-trace-isolate-and-quarantine under limited capacities

Julian Heidecke^{1,3,4}, Jan Fuhrmann², and Maria Vittoria Barbarossa^{*1}

¹Frankfurt Institute for Advanced Studies,

Ruth-Moufang-Straße 1, 60438 Frankfurt, Germany

²Institute of Applied Mathematics, Heidelberg University,
Im Neuenheimer Feld 205, 69120 Heidelberg, Germany

³Interdisciplinary Center for Scientific Computing, Heidelberg University,
Im Neuenheimer Feld 205, 69120 Heidelberg, Germany

⁴Heidelberg Institute of Global Health, Heidelberg University,
Im Neuenheimer Feld 130.3, 69120 Heidelberg, Germany

Abstract

Diagnostic testing followed by isolation of identified cases and subsequent tracing and quarantine of close contacts – often referred to as test-trace-isolate-and-quarantine (TTIQ) strategy – is one of the cornerstones of non-pharmaceutical infectious disease control. Non-pharmaceutical interventions are particularly important during the (re-)emergence of infectious diseases for which therapeutic drugs or vaccines are not yet available. The COVID-19 pandemic has highlighted that an appropriate response to outbreaks requires us to be aware about the effectiveness of such containment strategies. This can be evaluated using mathematical models. We present a delay differential equation model of TTIQ interventions for infectious disease control. Our model stands out from previous works through a detailed mechanistic description of the state-dependent dynamics induced by limited TTIQ capacities. In addition, we account for important disease characteristics that may be adverse to a TTIQ based control like presymptomatic transmissions. Numerical experiments reveal the effectiveness of TTIQ in the context of a scenario inspired by the second wave of COVID-19 infections in Germany in 2020 – representative of a situation where immunity within the population is low, pharmaceutical interventions are absent and identification of index cases by diagnostic testing and subsequent contact tracing are the main implemented measures in addition to contact restrictions and hygiene advices. Stability and sensitivity analyses emphasize factors, partially related to the specific disease, which impede or enhance the success of TTIQ. Studying the waning effectiveness of TTIQ along simulations of an epidemic wave we highlight consequences for intervention strategies.

Keywords— test-trace-isolate-and-quarantine, delay equations, COVID-19, limited capacities, sensitivity analysis, presymptomatic transmission

1 Introduction

In the absence of effective medication or vaccination, mitigation of an infectious disease relies on so called non-pharmaceutical interventions (NPIs) like mask mandates, hygiene measures, contact restrictions or test-trace-isolate-and-quarantine (TTIQ). These measures aim to reduce epidemiologically relevant contacts (*effective contacts*), viz., those between infectious and susceptible individuals during which the pathogen is successfully

*Corresponding author. Email: barbarossa@fias.uni-frankfurt.de

transmitted. In contrast to population-wide measures, TTIQ is directly targeted at individuals at risk of being infected. In principle, an effective implementation of TTIQ could allow to ease the need for population-wide contact restrictions and thereby reduce their socio-economic consequences. The TTIQ process begins with searching infected individuals within the population, potentially using some kind of laboratory *test* which is typically conducted symptom- or risk-based. Once detected, the so called index cases are asked to *isolate*¹ and information concerning their close contacts² is collected. Based on this information, attempts are then made to reach the close contacts (they are *traced*). Successfully approached close contacts are hence asked to self-*quarantine* for a period sufficient to cover their potential incubation and infectious phase. In this way, public health authorities (PHA) aim at catching infected individuals in an early phase, potentially asymptomatic or presymptomatic, in order to prevent further infections. From here on another round of contact tracing can be initiated by tracing contacts of contacts.

TTIQ is considered a cornerstone of infectious diseases control and was adopted by many countries worldwide to combat the spread of the coronavirus disease 2019 (COVID-19) caused by infection with severe acute respiratory syndrome coronavirus type 2 (SARS-CoV-2). However, its effectiveness is hampered by several factors. Some of these factors are inherent to the TTIQ process:

- Interviewing index cases about their close contacts and eventually approaching these requires time and results in the so called *tracing delay*.
- Limited capacities of PHA and testing laboratories cause the efficiency and speed of the TTIQ process to decrease if the prevalence of the considered disease, and thus the workload, increases.
- A variety of reasons can prevent individuals from complying with the PHA's request to participate in the TTIQ process.

Other limitations depend on the nature of the disease in question. For COVID-19 these include:

- The airborne transmission limits the proportion of identifiable infected contacts of any given detected infectious person, the so called *tracing coverage*, and implies that many potential contacts have to be traced per detected index case.
- Many infected individuals show weak or unspecific symptoms (they are paucisymptomatic) [1,2]. Moreover, there is a reportedly high proportion of presymptomatic transmissions [3–6]. This implies that a symptom-based testing strategy will lead to a limited *detection ratio* (the proportion of infectious individuals detected by testing before recovery) and a significant *testing delay* (the combined time between turning infectious, administration of a test, obtaining the test result and starting to isolate) has to be expected. Moreover, tracing the contacts of all symptomatic individuals, which might include many individuals with a common cold or other respiratory disease, is virtually impossible. Therefore, tracing usually has to be limited to the contacts of cases confirmed as infected through a polymerase chain reaction test.
- COVID-19 is associated with a relatively short latency period (time between infection and onset of infectiousness) and infectious period [3,6–10]. When the delays caused by testing and tracing become too large as compared to the timescale of disease progression, a small detection ratio is achieved and the contacts of an identified index case will already have caused infections themselves before they are successfully traced.

In light of these limitations, it is important to evaluate the contribution of TTIQ to disease mitigation and to assess how this depends on (i) disease characteristics and (ii) non-disease-specific factors like maintaining low prevalence (to prevent exhaustion of TTIQ capacities), or a high compliance with isolation mandates. To this end, mathematical modeling provides a powerful tool. However, incorporating TTIQ into standard mean-field models is challenging due to the individual-based character of contact tracing. Information about the timing, proximity and traceability of contacts of identified index cases has to be lifted from the individual-level to the population-level scale [11]. Moreover, in-host processes like the course of infectivity influence the population-level effect of TTIQ. To more readily include such fine grained mechanisms many models use agent- and network-based approaches [12–17],

¹In general we think here of domestic isolation and not particularly refer to hospital isolation, necessary in case of diseases with severe symptoms.

²Public health authorities provide criteria for defining close contacts, depending on available information on the transmissibility of the disease. This definition aims to target contact persons who have potentially been infected by the detected index cases.

or the corresponding branching process at the onset of the epidemic is studied [18–26]. Ordinary (ODE) and delay differential equation (DDE) models [27–34] are often less complex, allow for full simulation of the epidemic and are more amenable to analytical investigation. However, to derive quarantine rates in these simplified mean-field settings certain approximations have to be applied. Striking the right balance between an accurate representation of contact tracing and model simplicity is rather challenging. Several proposed models are based on simplistic approaches where contact tracing is represented by an increased removal rate of infectious individuals [30] or a certain fraction of the new close contacts is assumed to be instantly quarantined [33]. In more rigorous model formulations contact tracing is directly correlated to the identification of index cases [27, 34], though the efficiency of TTIQ is assumed to be independent of disease prevalence. In contrast, the model introduced in [29] accounts for limited TTIQ capacities assuming perfect efficiency until a certain prevalence/incidence is reached. The later was extended to account for a tracing delay which led to a model based on DDEs [28]. Another approach is presented in [32] where expressions for the probability that individuals had recent contact with an infectious individual are derived. This probabilistic argument is then used to derive tracing terms that aim at matching the individual- and population-level scales. The model is shown to be in good agreement with an agent-based model for most scenarios. The model in [31], which similarly to [28, 29] includes a limited testing capacity, focuses on contact heterogeneity by deploying a contact exposure distribution. Based on the idea of digital contact tracing, terms are derived to account for tracing of those contacts that are above a certain exposure threshold. This approach aims at finding an optimal notification threshold that manages to balance disease control and quarantine cost by minimizing unnecessarily quarantined contacts. Among those of the above ODE and DDE models that address COVID-19 [28–33], only the one in [31] explicitly accounts for presymptomatic transmissions, a key characteristic of infection with SARS-CoV-2. Models that keep track of the age of infection of infected individuals offer suitable frameworks to incorporate more realistic infectivity profiles and to derive exact contact tracing rates. Such age of infection approaches have been studied previously [4, 16, 25, 26, 35–37], considering also the effect of tracing delays [4, 25] or of limited capacities [37], yet again assuming perfect efficiency below a certain incidence threshold.

To aid knowledge and preparedness for future infectious disease outbreaks (COVID-19 or others) we find it necessary to refine and extend modeling approaches previously proposed in the literature. By means of an improved mean-field model we quantify the effectiveness of TTIQ in the context of COVID-19 and also identify factors that limit the success of this strategy. Our approach is based on mechanistic arguments and takes into account the various challenges TTIQ has to face. To consider limited laboratory testing capacity, we introduce state-dependent testing rates similar to those proposed in [38]. We derive contact tracing terms that link the success of index case identification to the quarantine rates achieved by contact tracing. The structure of the resulting terms is similar to those derived in [28], however, as with the testing terms, our model does not assume the contact tracing efficiency to be constant below a certain prevalence. Instead, the efficiency of testing and tracing is assumed to decrease smoothly with increasing prevalence due to limited capacity. Additionally, as for the model in [31] we account for presymptomatic transmission by introducing an infectious compartment of short duration in which individuals are already infectious but do not yet have an increased chance of being tested unless they are successfully traced. As a working example we consider a scenario inspired by the spread of COVID-19 in Germany during the second wave in late summer and fall of 2020. This specific situation is of interest for our study as in Germany (and many other European countries) an epidemic wave emerged after a summer of low prevalence, most of the population was still susceptible, pharmaceutical interventions were not widely available, and TTIQ was the main control measure applied in addition to population-wide hygiene and contact interventions. As such a situation is not unusual for (re-)emerging diseases focusing on this specific example does not restrict the general applicability of our results to other infectious diseases. Our modeling approach sheds light on what we can expect from TTIQ in this critical early phase of an epidemic and how its performance is impeded once case numbers begin to increase. Our results highlight implications for intervention strategies and underline conditions for an effective implementation of TTIQ.

2 Methods

2.1 Baseline SEIR model with testing

The core of the model used in this work extends the known *SEIR*-type model for disease dynamics [39]. The model comprises equations for compartments representing susceptible (S) individuals who can be infected, exposed

(E) individuals who are infected but not yet infectious, infectious (U and I) individuals who can spread the disease and removed (R) individuals who either recovered or died from the disease.

Infections might be confirmed (I) by testing previously undetected (U) individuals. Removed individuals are not involved in disease transmission, assuming permanent³ immunity upon recovery. Susceptible individuals can be infected via contacts with undetected (transmission rate β_U) or detected (β_I) infectious individuals. We assume that undetected infectious individuals, lacking knowledge about being infectious, do not restrict their contacts to others, and therefore have a higher transmission rate than detected infected individuals ($\beta_U > \beta_I$) who are expected to isolate themselves at least to some degree. The following system of differential equations describes the dynamics of these compartments:

$$\begin{aligned}\dot{S} &= -\lambda S \\ \dot{E} &= \lambda S - \alpha E \\ \dot{U} &= \alpha E - \eta_U U - \gamma U \\ \dot{I} &= \eta_U U - \gamma I \\ \dot{R} &= \gamma(U + I)\end{aligned}\tag{1}$$

with

$$\lambda = \frac{\beta_U U + \beta_I I}{N}$$

where $N = S + E + U + I + R$ denotes the total population size that is assumed to be constant⁴. We express the transmission rate of confirmed infectious individuals as

$$\beta_I = \rho_I \beta_U.$$

The parameter $\rho_I \in [0, 1]$ is the fraction of secondary infections caused per unit time by an average confirmed case as compared to an average undetected case. In this sense, ρ_I captures the efficiency of case isolation in reducing transmissions and the adherence with isolation. Disease progression is given by the rates α and γ , that is, $1/\alpha$ is the average duration of the latent period and $1/\gamma$ is the average duration of the infectious period. Detection of infectious individuals occurs at rate η_U . We assume that the detection rate is state-dependent and decreases for larger prevalence of infectious individuals due to finite testing capacity. More precisely, as motivated in [38], we set

$$\eta_U = \sigma_U \frac{\sigma_+}{S + \sigma_E E + \sigma_U U + \sigma_I I + \sigma_R R + \sigma_-},\tag{2}$$

where σ_+ is the maximal number of tests that can be administered and evaluated per unit time, σ_- describes the fact that lab capacity cannot be stored and goes to waste unless quickly used, and σ_X for $X \in \{E, U, I, R\}$ expresses the relative frequency of getting tested for individuals in compartment X relative to the respective frequency for susceptibles. Setting $\sigma_- = 0$ would correspond to full employment of available lab facilities by administering as many tests as can possibly be processed independent of the prevalence of the disease. It is reasonable to assume that $\sigma_U \gg 1$ meaning that the chance of being tested is significantly increased for infectious individuals, since these might show signs of being infected. This leads to a reasonably high detection rate at low prevalence, but as the prevalence rises the detection rate smoothly decreases, and an increased proportion of infections goes undetected. In contrast, a setting where $\sigma_X = 1$ for all $X \in \{E, U, I, R\}$ would correspond to a scenario where all available tests are used for randomly screening the population and leads to a constant but small detection rate of infections. In comparison to (2) a high and constant (that is, independent of the system's state) detection rate would lead to unrealistically high incidences of confirmed cases as the true prevalence increases.

³At least for the short simulation times under consideration.

⁴For simplicity, we neglect demographics including disease induced deaths.

2.2 Incorporation of contact tracing

In this section, we extend the baseline model presented in Section 2.1 by terms describing manual⁵ contact tracing. The process of contact tracing is initiated upon an infected individual being detected and confirmed by testing. Such positively tested index cases are interviewed in order to potentially identify (i) contacts they might have infected (*forward tracing*) and (ii) the individual that infected them (*backward tracing*). In this note we focus on the effect of forward tracing. This process is incorporated into the baseline model (1) based on the following assumptions:

- (A1) Contact tracing is triggered by confirmation of infectious cases by testing.
- (A2) Contact tracing is only triggered by confirmation of previously undetected infectious individuals ($U \rightarrow I$) (*first-order tracing*). More precisely, tracing contacts of contacts (*recursive tracing*), is neglected here.
- (A3) There is a fixed delay of κ units of time (here days) between the confirmation of an index case and the start of quarantine for their contacts. This delay represents the duration of the process of interviewing the index case and reaching out to close contacts.
- (A4) Although we assume them to be imperfectly isolated, index cases only share contacts made before their time in isolation.
- (A5) Individuals traced as contacts of a confirmed case are asked to quarantine themselves. Like for confirmed cases we assume that traced individuals are imperfectly quarantined. We suspect traced contacts that are not yet confirmed as infected by testing to reduce their contacts less strictly than confirmed cases.
- (A6) Only a certain fraction of secondary infections can be identified by PHA via contact tracing.
- (A7) PHA rely on limited capacities to conduct contact tracing.

In reality, all traced close contact persons, including those who did not get infected during their contact to the index case, are asked to quarantine⁶. This means that in practice many susceptible individuals would quarantine, but also that additional previously undetected infected persons (not necessarily infected by the index case above) could be found by chance. While we account for the tracing effort due to such contact persons, we do not explicitly consider the effects on the outbreak dynamics resulting from their quarantine.

To account for assumption (A5) we introduce two additional compartments, namely infected individuals detected by contact tracing who are still in the latency period (Q_E) and individuals detected by contact tracing who are already infectious and not yet confirmed through testing (Q_U). The transmission rate of individuals in Q_U is specified as

$$\beta_{Q_U} = \rho_Q \beta_U,$$

where $1 \geq \rho_Q > \rho_I$, meaning that traced individuals who are not yet confirmed as infected reduce their contacts less strictly than confirmed cases.

It is plausible to assume that the PHA strive to test all traced individuals during their quarantine to identify which of the reported contacts are indeed infected. Thus, we consider the rate at which these individuals are tested to be significantly larger than the corresponding rate for undetected infectious individuals $\sigma_{Q_U} \gg \sigma_U$. Following the reasoning in Section 2.1 we account for limited testing capacity by setting

$$\eta_U = \sigma_U \frac{\sigma_+}{S + \langle \sigma, X \rangle + \sigma_-}, \quad \eta_{Q_U} = \sigma_{Q_U} \frac{\sigma_+}{S + \langle \sigma, X \rangle + \sigma_-}, \quad (3)$$

where $\sigma = (\sigma_E, \sigma_{Q_E}, \sigma_U, \sigma_{Q_U}, \sigma_I, \sigma_R)$ and $X = (E, Q_E, U, Q_U, I, R)$. Being aware that η_U and η_{Q_U} are not constant but state dependent we usually omit this dependence in our notation and only specify $\eta_U(s)$ when referring to times in the past.

The above assumptions translate into the dynamics shown in Figure 1 and yield the following system of

⁵Manual means that the contact tracing strategy is based on PHA interviewing index cases to get information about close contacts. In contrast, digital contact tracing supports this process by using some kind of digital device that keeps track of contacts between individuals and can ideally notify close contacts instantly when index cases are confirmed as infected.

⁶At the time of contact notification, there is no way to pinpoint the truly infected contacts. Even if contacts quickly receive a laboratory test, some of them may still be in a phase where their infection is not yet detectable.

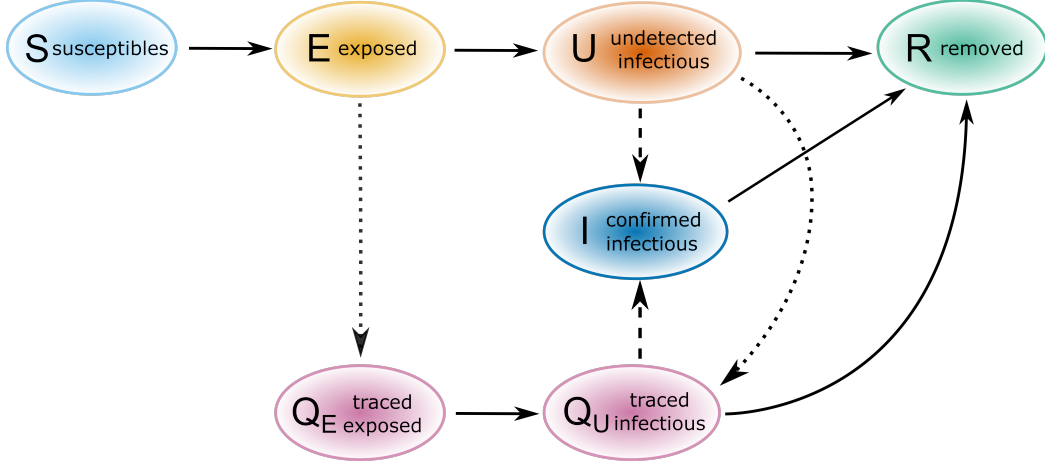


Figure 1: Model structure for the transmission dynamics of an infectious disease with TTIQ. Solid lines indicate state transitions due to disease spread and disease progression. Dashed lines indicate confirmation and isolation of infectious cases due to testing. Dotted lines indicate quarantine of infected contacts due to contact tracing.

differential equations

$$\begin{aligned}
\dot{S} &= -\lambda S \\
\dot{E} &= \lambda S - \alpha E - Tr_E \\
\dot{Q}_E &= Tr_E - \alpha Q_E \\
\dot{U} &= \alpha E - \eta_U U - \gamma U - Tr_U \\
\dot{Q}_U &= \alpha Q_E + Tr_U - \eta_{Q_U} Q_U - \gamma Q_U \\
\dot{I} &= \eta_U U + \eta_{Q_U} Q_U - \gamma I \\
\dot{R} &= \gamma(U + Q_U + I)
\end{aligned} \tag{4}$$

with

$$\lambda = \frac{\beta_U U + \beta_{Q_U} Q_U + \beta_I I}{N}.$$

It remains to explain the exact form of the terms Tr_E and Tr_U that describe the contact tracing process.

Assumptions (A1)-(A3) imply that the rate at which contacts are quarantined at time t is proportional to

$$\eta_U(t - \kappa)U(t - \kappa),$$

that is the rate at which detection of undetected infectious individuals (U to I) occurs at time $t - \kappa$. How does this term give rise to the rate at which contacts are quarantined at time t ? Consider an average index case confirmed as infectious by testing at time $t - \kappa$. We assume that for the interview of this index case the PHA use a certain *tracing window* T that determines the time interval

$$J_{t,T} := [t - \kappa - T, t - \kappa]$$

for which contacts of the index case are registered (*tracing interval*), neglecting that additional contacts made between time $t - \kappa$ and time t could also be reported (corresponding to assumption (A4)). Depending on the relationship between the tracing window T and the duration τ_t for which the average index case has been infectious by the time $t - \kappa$ of being detected⁷, the tracing interval $J_{t,T}$ is composed of two subintervals:

- the (potentially trivial) part of $J_{t,T}$ during which the index case was not yet infectious

$$J_{t,T}^{\text{minf}} := \begin{cases} \emptyset, & \text{if } T \leq \tau_t \\ [t - \kappa - T, t - \kappa - \tau_t], & \text{if } T > \tau_t, \end{cases}$$

⁷Approximation of τ_t is discussed in Appendix C. Notice that it is time-dependent due to limited TTIQ capacity.

- and the time in $J_{t,T}$ during which the index case has been infectious

$$J_{t,T}^{\text{inf}} := \begin{cases} [t - \kappa - T, t - \kappa], & \text{if } T \leq \tau_t \\ [t - \kappa - \tau_t, t - \kappa], & \text{if } T > \tau_t. \end{cases} \quad (5)$$

Moreover, we assume that PHA use a certain definition of close contact and ask the index case to report only contacts satisfying this definition. Along with the index case's ability to recall such contacts this determines

- \tilde{c}_1 , the reported close contact rate corresponding to the time interval $J_{t,T}^{\text{inf}}$,
- \tilde{c}_2 , the reported close contact rate corresponding to the time interval $J_{t,T}^{\text{inf}}$, and
- \tilde{p} , the infection probability corresponding to the close contacts made during $J_{t,T}^{\text{inf}}$.

On the one hand, it is reasonable to assume $\tilde{c}_2 \leq \tilde{c}_1$, since individuals in U might reduce their contacts when starting to show symptoms. On the other hand, this is countered by the fact that less recent contacts are harder to recall. Not trying to guess which of these effects is more pronounced, we work with the simplifying assumption $\tilde{c} := \tilde{c}_1 = \tilde{c}_2$. The product $\tilde{\beta} = \tilde{p}\tilde{c}$ determines the rate at which the index case produced traceable effective contacts in $J_{t,T}^{\text{inf}}$. Comparing $\tilde{\beta}$ with β_U and $|J_{t,T}^{\text{inf}}|$ with τ_t we have a proxy for the fraction of infected contacts covered by the contact tracing process (compare assumption (A6)). We call the fraction

$$\omega(t) = \frac{|J_{t,T}^{\text{inf}}| \tilde{\beta}}{\tau_t \beta_U} \leq 1 \quad (6)$$

the *tracing coverage* at time t . Social and hygiene measures obviously influence \tilde{c} , \tilde{p} , $\tilde{\beta}$. Moreover, the PHA might change their close contact definition over time or individuals might start to keep a contact diary to reduce recall issues. We discuss how we handle such measures and time-dependent parameters in Appendix B. A possible timeline of events for an index case detected at time $t - \kappa$ by testing whose contacts are quarantined at time t is shown in Figure 2.

Following the above assumptions we approximate the rate at which contacts become traceable at time t as

$$c_{\text{pot}}(t) = |J_{t,T}| \tilde{c} \eta_U(t - \kappa) U(t - \kappa). \quad (7)$$

Due to limited resources that can be provided to conduct contact tracing (compare assumption (A7)) not all traceable contacts necessarily end up being successfully contacted and quarantined. We assume an upper bound Ω (*tracing capacity*) for the actual rate at which contacts are quarantined due to contact tracing. As a rough approximation we could choose

$$c_{\text{act}}(t) = \min(\Omega, c_{\text{pot}}(t)) \quad (8)$$

for the actual rate at which contacts are quarantined at time t . However, we suppose the *tracing efficiency*⁸ to be continuously decreasing as the number of traceable contacts increases. That is, we assume that almost perfect efficiency corresponding to the assumed tracing delay can only be achieved for small rates of traceable contacts. For this reason, we smooth (8) by a saturating function of the form

$$c_{\text{act}}(t) = c_{\text{pot}}(t) \frac{\Omega}{\underbrace{(c_{\text{pot}}(t)^p + \Omega^p)^{1/p}}_{=: \varepsilon(t) \text{ tracing efficiency at time } t}}, \quad p > 0. \quad (9)$$

As shown in Figure 3, a larger choice of p corresponds to a slower initial decrease in tracing efficiency as $c_{\text{pot}}(t)$ rises whereby the limit case $p \rightarrow \infty$ gives

$$\varepsilon(t) = \frac{\Omega}{\|(c_{\text{pot}}(t), \Omega)\|_{\infty}}$$

⁸The tracing efficiency denotes the share of successfully traced contacts among all traceable contacts while maintaining the constant tracing delay κ . In this sense the tracing efficiency in our model can be seen as the fraction of the theoretical tracing coverage that is indeed achieved in practice under consideration of the current load on capacities.

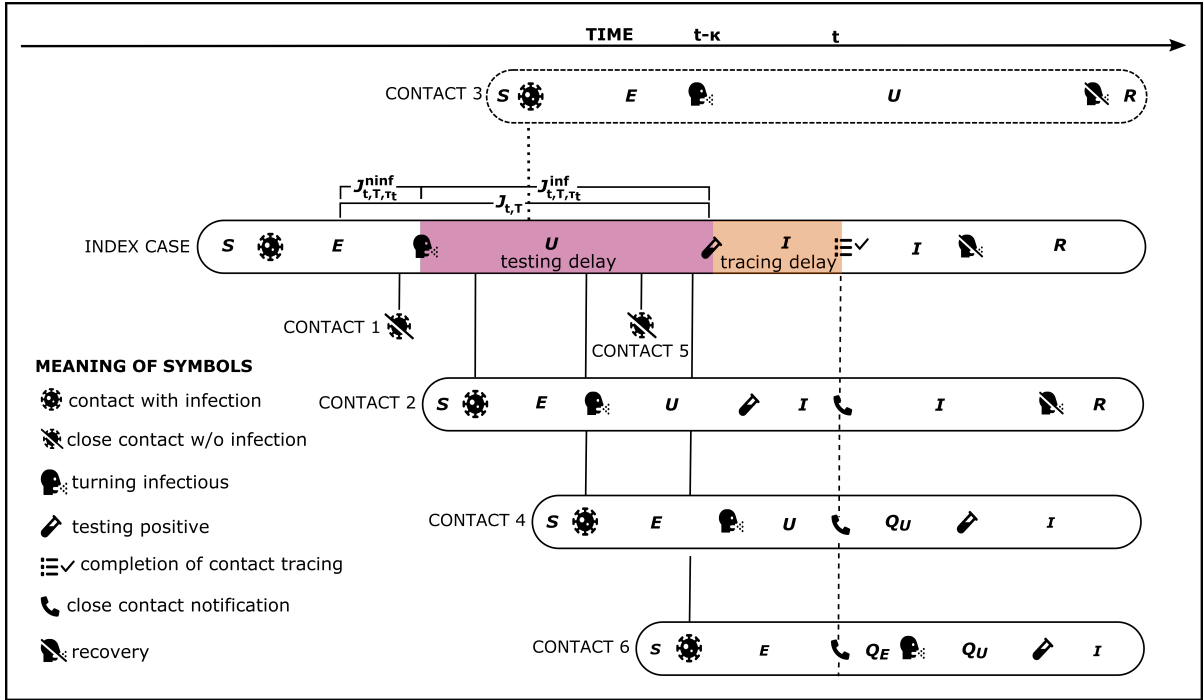


Figure 2: Possible timeline of events for an index case detected by testing at time $t - \kappa$ and contacts made during the tracing interval $J_{t,T}$ for which the index case is asked to share close contacts from. The tracing window, the testing and tracing delay, the close contact definition and the index cases ability to recall close contacts determine the effectiveness of contact tracing and the associated workload. In the depicted example the tracing interval $J_{t,T}$ is longer than the testing delay resulting in Contact 1 being reported although it could not have been infected since the index case was not yet infectious. Contact 2 gets infected early during the infectious phase $J_{t,T}^{inf}$ of the tracing interval and the time lag resulting from the testing and tracing delay lead to it being already confirmed by testing by the time t of being notified to be a close contact. Contact 3 is an example of an individual that got infected but is missed by the tracing process. This might happen because the contact is not covered by the close contact definition or cannot be recalled by the index case. Contact 4 and Contact 6 get infected late in $J_{t,T}^{inf}$, shortly before the index case is confirmed as infectious by testing. Therefore, these contacts are less affected by the testing delay, leading to Contact 4 being undetected but infectious and Contact 6 even being still latent by the time of being traced t . Contact 5 falls under the definition of being a close contact to the index case and is therefore traced even though no transmission took place. We account for the tracing effort such contacts generate in the tracing efficiency, however we do not consider their quarantine in our model.

which exactly corresponds to (8). Several factors determine whether the tracing efficiency can be kept high when the prevalence rises (large p) or whether it is quickly diminished (small p). These include the ease with which additional workforce can be recruited and the efficiency at which this additional workforce (that may be trained for a different purpose) operates. Moreover, when considering an epidemic outbreak in a large area, the outbreak is usually spatially heterogeneous across different regions, with some regions more affected than others. The tracing efficiency can only be kept high in regions with high prevalence when capacity from low prevalence regions can easily be shifted there. If this is not the case (low p), then severely affected regions already have low tracing efficiency although the overall prevalence in the considered area might still be relatively low. In a mean-field model like (4) this is reflected in a fast decreasing tracing efficiency as prevalence rises. As the infection continues to spread, the outbreak is likely to approach states of high prevalence in all regions. As soon as the pool of additionally recruitable workforce is used up, it is plausible to assume that the considered area makes use of its total capacity and a maximal rate at which contacts can be quarantined is approached.

Only the susceptible close contacts made in the time interval $J_{t,T}^{inf}$ can have been infected by the index case.

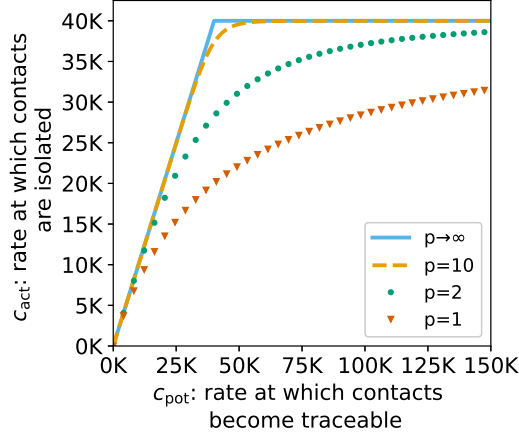


Figure 3: Illustration of relation (9) for the choice $\Omega = 40000$ and multiple values of p . The limit $p \rightarrow \infty$ recovers relation (8). Mind the different scaling of the axes.

The rate at which actually infected contacts are quarantined at time t is therefore

$$c_{\text{act}}^{\text{inf}}(t) = \frac{|J_{t,T}^{\text{inf}}|}{|J_{t,T}|} \tilde{p} \frac{S(t-\kappa)}{N} c_{\text{act}}(t). \quad (10)$$

Notice that here we approximate the fraction of susceptible individuals to be constant in the short time interval $J_{t,T}^{\text{inf}}$. Plugging (9) into (10), using (7) and $\tilde{\beta} = \tilde{p}\tilde{c}$ we get

$$\underbrace{c_{\text{act}}^{\text{inf}}(t)}_{\text{actual rate at which infected contacts are quarantined at time } t} = \underbrace{\frac{|J_{t,T}^{\text{inf}}| \tilde{\beta}}{|J_{t,T}|}}_{\text{secondary infections reported by an average index case that was isolated at time } t-\kappa} \underbrace{\frac{S(t-\kappa)}{N}}_{\text{rate of index case identification at time } t-\kappa} \underbrace{\eta_U(t-\kappa)U(t-\kappa)}_{\text{rate of index case identification at time } t-\kappa} \underbrace{\varepsilon(t)}_{\text{tracing efficiency at time } t}. \quad (11)$$

Using our proxy (11) for the actual rate at which infected contacts are quarantined at time t we can now determine $Tr_E(t)$ and $Tr_U(t)$. Following a similar reasoning as in [28], we can approximate the fraction of (11) originating from the exposed or infectious stage. Let us again consider the average index case detected at time $t - \kappa$ by testing. Infection of close contacts reported by this index case took place during $J_{t,T}^{\text{inf}}$ and by the time of being quarantined all of these contacts are infected for at least a duration of κ units of time due to the tracing delay. Approximating the infection events produced by our average index case to be uniformly distributed on $J_{t,T}^{\text{inf}}$ we estimate the time an average infected contact spent in the infected chain by the time t of being quarantined as

$$\tilde{r}(t) = \kappa + \frac{1}{2}|J_{t,T}^{\text{inf}}|. \quad (12)$$

A fraction

$$\mu_E(t) := \exp(-\alpha\tilde{r}(t))$$

of successfully traced individuals infected by the index case remains in the exposed state ($E \rightarrow Q_E$) after $\tilde{r}(t)$ units of time in the infected chain. The remaining fraction described by the term $1 - \mu_E(t)$ have entered the U -compartment but might have been tested themselves or might have recovered by the time of being traced. Therefore, to approximate the fraction of quarantined infected contacts coming from the infectious stage ($U \rightarrow Q_U$) we keep following the first-order kinetics of system (4) and solve

$$\frac{d\tilde{U}}{ds} = -(\gamma + \eta_U(t-\kappa))\tilde{U} + \alpha \exp(-\alpha s), \quad \tilde{U}(0) = 0 \quad (13)$$

Table 1: Dynamic variables of the full model (14).

Notation	Description
S	susceptible individuals
E	undetected exposed individuals
Q_E	traced and quarantined exposed individuals
U_1	undetected presymptomatic infectious individuals
Q_{U_1}	traced and quarantined presymptomatic infectious individuals
I_1	confirmed and isolated presymptomatic infectious individuals
U_2	undetected symptomatic infectious individuals
Q_{U_2}	traced and quarantined symptomatic infectious individuals
I_2	confirmed and isolated symptomatic infectious individuals
R	removed individuals

up to time $s = \tilde{r}(t)$. Notice that we here assume the testing rate $\eta_U(t - \kappa)$ to be approximately constant in the short time interval $|\tilde{J}_{t,T}^{\text{inf}}|$. The solution to the initial value problem (13) evaluated at time $s = \tilde{r}(t)$ is given by⁹

$$\mu_U(t) := \tilde{U}(\tilde{r}(t)) = \frac{\alpha}{\eta_U(t - \kappa) + \gamma - \alpha} (\exp(-\alpha\tilde{r}(t)) - \exp(-(\eta_U(t - \kappa) + \gamma)\tilde{r}(t))).$$

This motivates us to set

$$Tr_E(t) = \mu_E(t)c_{\text{act}}^{\text{inf}}(t) \quad \text{and} \quad Tr_U(t) = \mu_U(t)c_{\text{act}}^{\text{inf}}(t).$$

2.3 Presymptomatic transmissions

The proportion of transmission occurring prior to symptom onset has been shown before to be a critical quantity for the success or failure of TTIQ [35]. To account for the reportedly high proportion of presymptomatic transmissions in case of infection with SARS-CoV-2 [3–6] we extend model (4) in the following by a presymptomatic infectious phase.

We start by splitting each infectious compartment (U, Q_U, I) into two compartments $(U_1, U_2, Q_{U_1}, Q_{U_2}, I_1, I_2)$ where all compartments with index 1 belong to the presymptomatic phase. Individuals in the compartments with index 2 are beyond that initial phase. We call these individuals *symptomatic* although it should be stressed that these compartments, especially U_2 , might comprise individuals with widely varying degrees of symptom severity. While all the individuals in, e.g. U_1 , are asymptomatic, hence unlikely to be tested, a certain fraction of individuals in U_2 show specific symptoms leading to a significantly higher testing rate in this compartment $\eta_{U_2} \gg \eta_{U_1}$. We denote the average duration of the presymptomatic phase by $1/\gamma_1$. The average duration of the symptomatic period is denoted by $1/\gamma_2$. The parameter β_{U_1} (β_{U_2}) refers to the transmission rate at which presymptomatic (symptomatic) undetected infectious individuals spread the disease. We assume that $\beta_{U_1} = \theta\beta_{U_2}$ for some scaling factor θ describing the extent of early viral shedding. For simplicity, the factor p_Q (p_I), which describes the strictness of quarantine (isolation) of traced (confirmed) infectious cases, is assumed to reduce the transmission rates of individuals in Q_{U_1} and in Q_{U_2} (I_1 and I_2) to the same extent. All the system state variables as well as their meanings are summarized in Table 1.

A sketch of the dynamics described by the following system of differential equations is given in Figure 4

⁹The solution continuously extends to $\mu_U(t) = \alpha\tilde{r}(t)\exp(-\alpha\tilde{r}(t))$ in the degenerate case $\alpha = \eta_U(t - \kappa) + \gamma$.

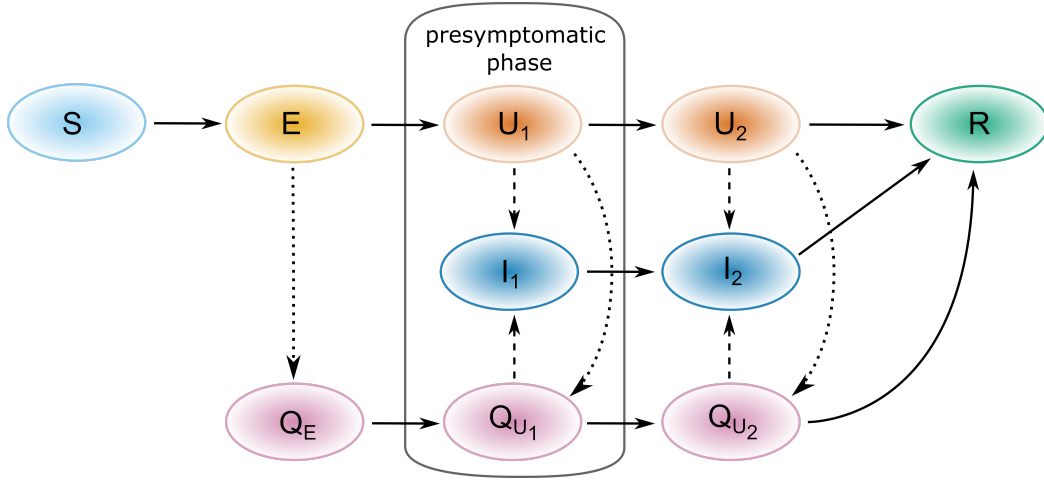


Figure 4: Model structure that extends the dynamics shown in Figure 1 by a presymptomatic phase. Solid lines indicate transitions due to disease spread and disease progression. Dashed lines indicate detection and isolation of infectious cases due to testing. Dotted lines indicate quarantine of infected contacts due to contact tracing.

$$\begin{aligned}
\dot{S} &= -\lambda S \\
\dot{E} &= \lambda S - \alpha E - Tr_E \\
\dot{Q}_E &= Tr_E - \alpha Q_E \\
\dot{U}_1 &= \alpha E - \eta_{U_1} U_1 - \gamma_1 U_1 - Tr_{U_1} \\
\dot{Q}_{U_1} &= \alpha Q_E + Tr_{U_1} - \eta_{Q_{U_1}} Q_{U_1} - \gamma_1 Q_{U_1} \\
\dot{I}_1 &= \eta_{U_1} U_1 + \eta_{Q_{U_1}} Q_{U_1} - \gamma_1 I_1 \\
\dot{U}_2 &= \gamma_1 U_1 - \eta_{U_2} U_2 - \gamma_2 U_2 - Tr_{U_2} \\
\dot{Q}_{U_2} &= \gamma_1 Q_{U_1} + Tr_{U_2} - \eta_{Q_{U_2}} Q_{U_2} - \gamma_2 Q_{U_2} \\
\dot{I}_2 &= \eta_{U_2} U_2 + \eta_{Q_{U_2}} Q_{U_2} + \gamma_1 I_1 - \gamma_2 I_2 \\
\dot{R} &= \gamma_2 (U_2 + Q_{U_2} + I_2)
\end{aligned} \tag{14}$$

with

$$\lambda = \frac{\beta_{U_1} U_1 + \beta_{U_2} U_2 + p_Q (\beta_{U_1} Q_{U_1} + \beta_{U_2} Q_{U_2}) + p_I (\beta_{U_1} I_1 + \beta_{U_2} I_2)}{N}.$$

The contact tracing terms Tr_E, Tr_{U_1}, Tr_{U_2} are derived similarly as we proceeded for the model with uniform infectious phase in Section 2.2. However, in the presence of a presymptomatic infectious period we distinguish between index cases detected by testing while being in U_1 and U_2 , respectively. The derivation of the associated tracing terms is quite lengthy and described in detail in Appendix A.

2.4 Modeling of social and hygiene measures and assessment of TTIQ effectiveness

We briefly describe how population-wide social and hygiene measures are modeled and how we evaluate the effectiveness of TTIQ. For a detailed description on how we account for the effect of contact measures on the contact tracing terms we refer to Appendix B.

Population-wide contact measures are modeled by a time dependent factor $\phi(t) \in [0, 1]$, that scales the transmission rates, i.e.,

$$\beta_{U_2}(t) = \phi(t) \overline{\beta_{U_2}},$$

where $\overline{\beta_{U_2}}$ is the baseline transmission rate of individuals in the undetected symptomatic stage corresponding to a phase without any intervention. In case of COVID-19, this can be seen as the transmission rate that would

be observed given our contact level before (or in a very early phase during) the first occurrence of the disease¹⁰. Thus, this baseline transmission rate is associated to the basic reproduction number by

$$\mathcal{R}_0 = \frac{\theta \overline{\beta_{U_2}}}{\gamma_1} + \frac{\overline{\beta_{U_2}}}{\gamma_2}. \quad (15)$$

The factor $\phi(t)$ can be seen as the level of effective contacts at time t compared to the "pre-COVID-19" scenario and leads to the control reproduction number

$$\mathcal{R}_c := \phi \mathcal{R}_0.$$

Let ϕ^* denote the maximal level of effective contacts for which the disease-free equilibrium (DFE), $(N, 0, \dots, 0)$, is stable. In the absence of TTIQ this is clearly given by

$$\phi^* = \frac{1}{\mathcal{R}_0}. \quad (16)$$

In the presence of TTIQ we can derive ϕ^* from a numerical stability analysis of the DFE (see Appendix D for details). This allows to assess the effectiveness of TTIQ at low prevalence. The higher the obtained ϕ^* , the better the performance of TTIQ and the lower the need for social and hygiene measures. Additionally, comparison to the value obtained in the absence of TTIQ (16) gives a measure of how much population-wide contact restrictions can be relaxed thanks to TTIQ. For a given TTIQ scenario and the corresponding ϕ^* we can also interpret

$$\mathcal{R}_c^{\max} := \phi^* \mathcal{R}_0 \quad (17)$$

as the maximal control reproduction number that can be contained by the given TTIQ effort. Later, we also consider scenarios with high prevalence that operate far from the disease-free state, such that stability of the DFE does not offer sufficient information for disease control. Therefore, in these cases we evaluate the effectiveness of TTIQ based on $\bar{\phi}$, which we define as the maximum level of effective contacts that achieves stagnation in the incidence of infected individuals. Clearly, at low prevalence (and low immunization) we have $\bar{\phi} \approx \phi^*$.

We remark that both ϕ^* and $\bar{\phi}$ (and the corresponding values of TTIQ parameters) are threshold values that ensure stability of the DFE or the incidence of infected individuals (i.e., achieve $\mathcal{R}_t \approx 1$). However, in reality the aim is usually to reduce \mathcal{R}_t to a specified value below 1. Therefore, the derived parameter values should be interpreted as minimally required efforts. In particular, operating at or slightly below $\mathcal{R}_t = 1$ would come with the risk of minor changes in some external parameters driving \mathcal{R}_t above 1, initiating a new wave of exponentially increasing case loads.

3 Results

In this section we apply our model (14) to investigate the effectiveness of TTIQ in disease control. As a working example of a disease spreading in a population with low immunity, we consider the early spread of COVID-19 in Germany. For this framework, we defined a baseline parameter setting that is motivated in detail in Supplement C and summarized in Table 2. We start by considering the dynamics near the DFE, where the effect of TTIQ is barely curtailed by limited capacity. Studying the sensitivity of our results to parameter changes reveals the disease- and non-disease-specific factors influencing the performance of TTIQ. We then turn to the situation of an epidemic outbreak. We study the capacity-related declining impact of TTIQ as prevalence rises. Revisiting parameter changes reveals implications for intervention strategies.

Performance of TTIQ near the DFE

We compared values of the maximum level ϕ^* of effective contacts for which the DFE is stable (explained in Section 2.4) for (i) a scenario without TTIQ, (ii) a scenario in which only testing is performed, and (iii) a scenario in which both testing and contact tracing are performed (Figure 5A). In our baseline setting we assume $\mathcal{R}_0 = 3.3$, and thus, get $\phi^* \approx 0.304$ in the absence of TTIQ from relation (16). Adding testing activity controls the disease

¹⁰For the short simulations considered, we assume $\overline{\beta_{U_2}}$ to be constant and thereby ignore viral evolution over time.

Table 2: Parameters of the full model (14) including presymptomatic transmissions. The given values describe our baseline setting and are motivated in Appendix C.

Notation	Description	Value	Units
$\overline{\beta_{U_2}}$	baseline transmission rate of symptomatic undetected individuals	0.33	days ⁻¹ people ⁻¹
θ	scaling factor for transmission rate in presymptomatic period	1.5	dimensionless
(p_Q, p_I)	strictness of quarantine and isolation	(0.2, 0.1)	dimensionless
α	exposed to infectious rate	1/3.5	days ⁻¹
γ_1	presymptomatic to symptomatic rate	1/2	days ⁻¹
γ_2	symptomatic to removed rate	1/7	days ⁻¹
σ_+	maximal number of tests administered and evaluated per day	200 000	days ⁻¹ tests
σ_-	decay rate of tests	1.353 N	days ⁻¹
(σ_{U_2}, σ_Q)	relative frequency of testing undetected symptomatic and traced individuals compared to susceptibles	(93, 300)	people ⁻¹ days ⁻¹
T	tracing window	9	days
\bar{c}	baseline reported close contact rate	0.8	days ⁻¹ people ⁻¹
ω	tracing coverage	0.65	dimensionless
Ω	maximal contact quarantine rate	40 000	days ⁻¹ people
κ	tracing delay	2	days
p	tracing efficiency constant	2	dimensionless
N	population size	83 000 000	people

at higher rates of effective contacts $\phi^* \approx 0.407$. The addition of contact tracing to testing further increases the maximum level of effective contacts that provides stability of the DFE to $\phi^* \approx 0.461$. These values for ϕ^* correspond to a maximal control reproduction number that can be contained (see relation (17)) of at most $\mathcal{R}_c^{\max} \approx 1.34$ when only testing is applied and $\mathcal{R}_c^{\max} \approx 1.52$ when the full TTIQ approach is applied¹¹. This shows that in our baseline setting (i) the full TTIQ approach allows for an approximately 52% higher effective contact rate, (ii) testing contributes more to disease control than contact tracing and (iii) even in the presence of both testing and contact tracing a quite severe reduction of effective contacts by other measures to 46% of the pre-COVID-19 level is needed.

Sensitivity to TTIQ parameters

To determine the most influential TTIQ parameters on ϕ^* , we first considered single parameters one after the other and varied them in ranges according to Table 3 (Figure 6). As shown in Figure 6A, weak isolation of confirmed

¹¹That means that if the reproduction number would be brought to less than 1.34 by social and hygiene measures, testing alone would be sufficient to suppress an outbreak, and if it were lower than 1.52, the full TTIQ approach without further contact reduction measures could prevent an outbreak – assuming that the prevalence were still sufficiently low (that is the dynamics were yet close to the DFE).

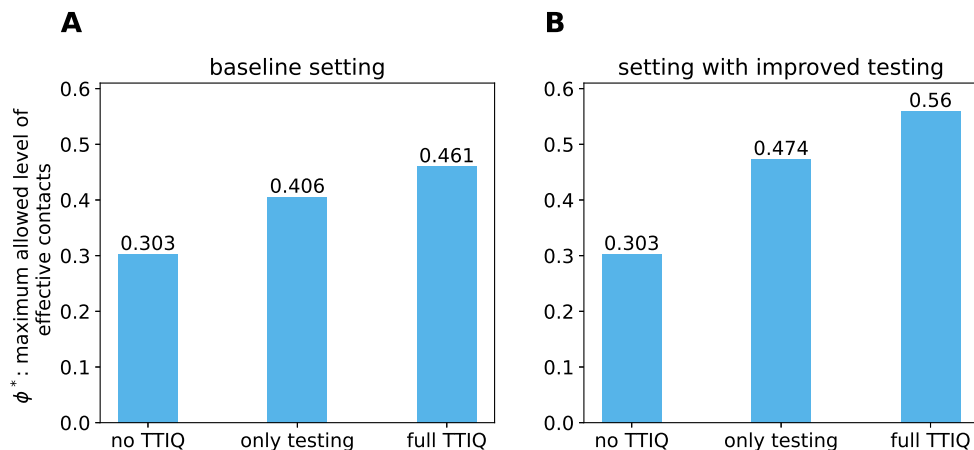


Figure 5: Maximum level ϕ^* of effective contacts for which the DFE is stable for a scenario without any TTIQ (no TTIQ), a scenario where only testing is conducted (only testing) and a scenario where testing and tracing is carried out (full TTIQ) in **A** the baseline setting given in Table 2 and **B** a setting with improved testing such that $\sigma_{U_2} = 185$.

Table 3: TTIQ parameter ranges considered in the sensitivity analysis.

parameter	meaning	range
ω	tracing coverage	$[0, 1]$
σ_{U_2}	relative frequency of testing undetected symptomatic individuals	$[1, 186]$
σ_Q	relative frequency of testing traced individuals	$[1, 600]$
p_Q	strictness of quarantine	$[0, 1]$
p_I	strictness of isolation	$[0, 1]$
κ	tracing delay	$[0.5, 14]$

infectious cases I (p_I close to 1) leads to $\phi^* \approx 0.304$, thus, renders TTIQ completely ineffective. Contact tracing is dependent on prior index case identification and is more effective the shorter the testing delay. This explains why improving testing has the side effect of increasing the effectiveness of contact tracing (compare Figure 5A where $\sigma_{U_2} = 93$ vs. Figure 5B where $\sigma_{U_2} = 185$) and why the relative frequency σ_{U_2} of testing undetected infectious individuals has a significantly larger impact on ϕ^* than the parameters associated with contact tracing ($\omega, \kappa, \sigma_Q, p_Q$) (compare Figure 6B with Figure 6C, Figure 6D and Figure 6E). The tracing coverage ω appears to be slightly more important than the tracing delay κ (compare Figure 6C, Figure 6D). This, however, is mainly due to the baseline parameters we chose, with a relatively short tracing delay $\kappa = 2$ and only moderate tracing coverage $\omega = 0.65$. Either of these parameters being in an unfavorable range severely limits the effect of any change of the other. In particular, in a setting with long tracing delay but high coverage it is the other way around (not shown here). The strictness of quarantine p_Q of traced but not yet tested individuals as well as the relative frequency σ_Q at which these individuals are tested appear to have no significant effect (Figure 6E-F). However, it should be noticed that we chose quite optimistic values for p_Q and σ_Q in our baseline setting (Table 2). Clearly, p_Q becomes more important when σ_Q is smaller and σ_Q gains importance when p_Q is close to unity (Figure 7A)¹². Simultaneous improvements of other parameters show synergistic effects. For example stricter

¹²In reality σ_Q may be of higher importance as it enables recursive tracing by identifying truly infected contacts. This process is neglected in our equations.

ϕ^* : maximum allowed level of effective contacts

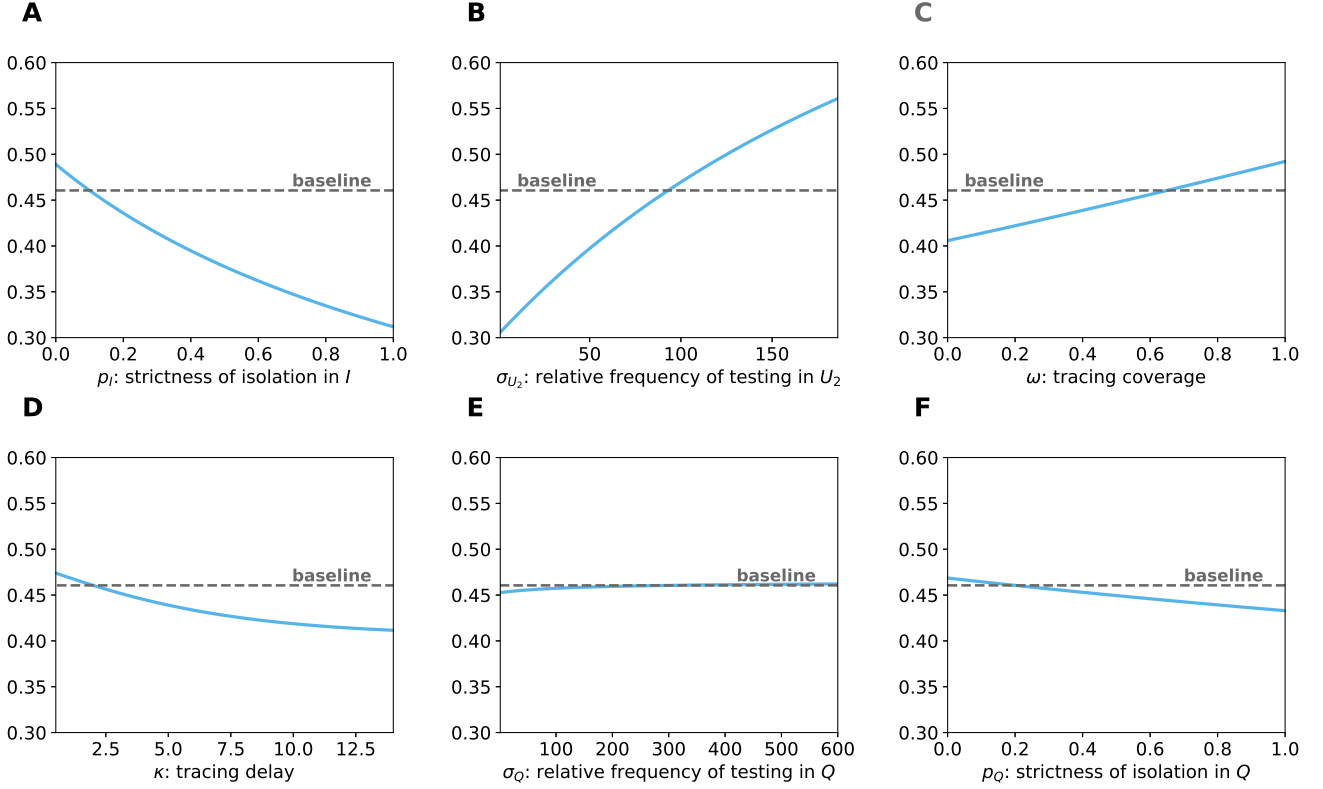


Figure 6: Maximum level ϕ^* of effective contacts that provides stability of the DFE (solid lines) in dependence of single TTIQ parameters. For comparison we also show the value of ϕ^* derived from our baseline parameter setting (dashed line) given in Table 2.

isolation and quarantine reinforce the benefits of improved testing (Figure 7B), a similar effect is present between improving tracing coverage and improving testing (Figure 7C), or, between improvements of tracing coverage and tracing delay (Figure 11A).

To gain insight on the global sensitivity of ϕ^* we used latin hypercube sampling on the TTIQ parameter space as given in Table 3 and calculated the corresponding partial rank correlation coefficients (PRCCs). This allows us to visualize which TTIQ parameters are most influential on ϕ^* , even if other parameters are simultaneously perturbed [40]. We excluded strictness of quarantine p_Q of traced contacts from this analysis to rule out the unnatural cases $p_Q < p_I$ in which traced (but so far unconfirmed) cases reduce their contacts more strictly than confirmed cases¹³. Instead we allowed p_I and all the remaining parameters given in Table 3 to vary and set

$$p_Q = \begin{cases} 2p_I, & p_I < 0.5 \\ 1, & \text{else.} \end{cases}$$

The calculated PRCCs support our observations from the variation of single parameter values. The strictness of isolation p_I of confirmed cases is predicted to be most influential on ϕ^* having the largest PRCC (absolute), closely followed by the relative frequency σ_{U_2} of testing undetected symptomatic individuals which is associated with a significantly larger PRCC than all the parameters corresponding to contact tracing ω, κ, σ_Q (Figure 8).

¹³In these cases increases in σ_Q would be predicted to have negative impact on ϕ^* .

ϕ^* : maximum allowed level of effective contacts

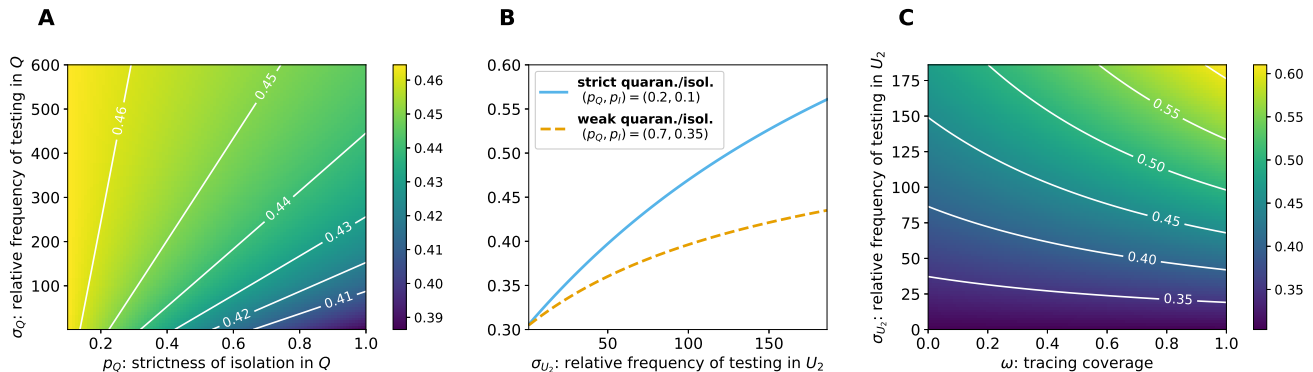


Figure 7: Maximum level ϕ^* of effective contacts that provides stability of the DFE in dependence of **A** the strictness of quarantine p_Q and the relative frequency σ_{Q_U} of testing traced contacts, **B** the relative frequency σ_{U_2} of testing undetected symptomatic individuals assuming either strict quarantine and isolation $(p_Q, p_I) = (0.2, 0.1)$ (solid line) or weak quarantine and isolation $(p_Q, p_I) = (0.7, 0.35)$ (dashed line) and **C** the relative frequency σ_{U_2} of testing undetected symptomatic individuals and the tracing coverage ω .

Impact of disease characteristics

We considered variations in parameters describing disease characteristics to gain insights on how the effectiveness of TTIQ might be changed for other infectious diseases and to investigate potential uncertainty regarding our parameter choices. All parameter changes studied below ensure that \mathcal{R}_0 is kept constant, according to formula (15). In particular, the maximal allowed level ϕ^* of effective contacts in the absence of TTIQ (compare equation (16)) stays unchanged and all deviations in ϕ^* can be attributed to increased or decreased TTIQ effectiveness.

A high incidence of asymptomatic or paucisymptomatic infectious individuals implies a reduced frequency of testing in compartment U_2 which we demonstrated to have a major impact on the maximum level ϕ^* of effective contacts that provides stability (Figure 6B). Therefore, TTIQ has to be expected significantly more effective if overt symptoms occur frequently upon infectious individuals.

Presymptomatic transmission is characterized by the average length of the presymptomatic period $1/\gamma_1$, and by the scaling factor θ of the presymptomatic transmission rate. We investigated the effects of variations in these parameters on ϕ^* . When varying $1/\gamma_1$ we adjusted $1/\gamma_2$ such that we maintain the same average for the total duration of the infectious period $1/\gamma = 1/\gamma_1 + 1/\gamma_2$, and adjusted the transmission rates in order not to alter \mathcal{R}_0 . Both larger $1/\gamma_1$ and larger θ increase the amount of transmissions that cannot be prevented by symptom-based testing. Larger $1/\gamma_1$ additionally implies a smaller detection ratio achieved by testing (at least if $1/\gamma_1 + 1/\gamma_2$ and σ_{U_2} stay unchanged) and a larger testing delay resulting in traced contacts having spent more time in the chain of infection before being quarantined. As shown in Figure 9, variations in both parameters notably affect the maximum allowed level ϕ^* of effective contacts.

To assess the sensitivity of TTIQ to the time scale of disease spread, we also considered changes in the mean duration of the latent period $1/\alpha$ and the mean duration of infectious phase $1/\gamma = 1/\gamma_1 + 1/\gamma_2$. When varying $1/\gamma$ we adjusted the transmission rate to maintain the same basic reproduction number \mathcal{R}_0 and kept a constant ratio between γ_1 and γ_2 such that the proportion of transmissions occurring in the presymptomatic phase in the absence of TTIQ remains unchanged. Unsurprisingly, faster disease progression (smaller $1/\alpha$, $1/\gamma$) leads to a smaller maximum allowed level ϕ^* of effective contacts (Figure 10). A longer latency period (larger $1/\alpha$) implies that more infected contacts are still latent at the time of being traced and thus more onward transmissions are prevented by their quarantine. This only affects the effectiveness of contact tracing and has no effect on a purely testing-based scenario (compare second bars in Figure 10B-E). Larger $1/\gamma$ increases the detection ratio achieved by testing (at least if σ_{U_2} stays unchanged) and implies that less traced contacts will have recovered by the time of being quarantined. Figure 10B-E demonstrates that this increases the benefit of both testing and contact tracing.

We found that disease characteristics not only influence ϕ^* directly but also its sensitivity with respect to the TTIQ parameters. For instance, the tracing delay (at least for the values considered here) gains relevance when compared to the tracing coverage in case of a shorter latent phase (compare slope of contour lines in Figure 11B

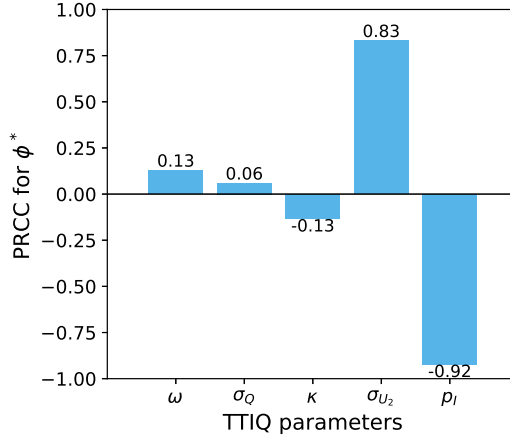


Figure 8: Global sensitivity of the maximum level ϕ^* of effective contacts that provides stability of the DFE with respect to TTIQ parameters as given by PRCCs obtained from latin hypercube sampling from the parameter space specified in Table 3.

ϕ^* : maximum allowed level of effective contacts

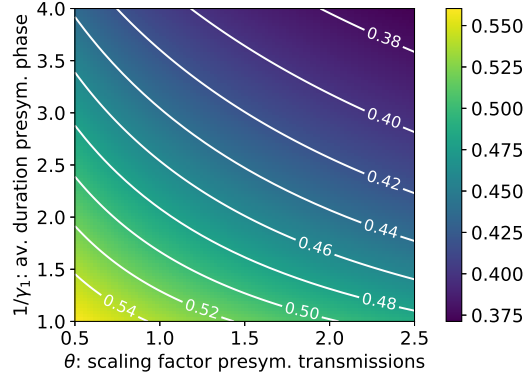


Figure 9: Maximum level ϕ^* of effective contacts that provides stability of the DFE in dependence of the average duration of the presymptomatic period $1/\gamma_1$ and the scaling factor θ of the presymptomatic transmission rate.

and Figure 11C).

Loss of control during outbreak

When prevalence rises the effectiveness of testing and tracing decreases and our stability analysis about the DFE does not offer sufficient information for disease control. To investigate how the effectiveness of TTIQ is affected by high prevalence, we considered a scenario where we assume moderately effective contact measures that are insufficient to control disease spread at the DFE ($\phi = 0.6 > 0.46 \approx \phi^*$). We initiate the simulation near the DFE and choose initial data¹⁴ as

$$(S, E, Q_E, U_1, Q_{U_1}, I_1, U_2, Q_{U_2}, I_2, R)(0) = (82\,975\,287, 2\,564, 131, 1\,301, 86, 52, 2\,173, 207, 1\,666, 16\,533).$$

Although not being an exact representation, this setting is qualitatively resembling the surge in cases in late summer and early fall of 2020 in Germany: most of the population is still susceptible¹⁵, the simulation starts at a

¹⁴More precisely, to initialize a system of delay differential equations, we have to choose a certain history function. Here we initialize all simulations with constant history functions.

¹⁵We do not claim that the initial data exactly represent the existing immunity within the German population as of summer 2020. Our exact choice was simply made to align the system to its leading eigenvector.

ϕ^* : maximum allowed level of effective contacts

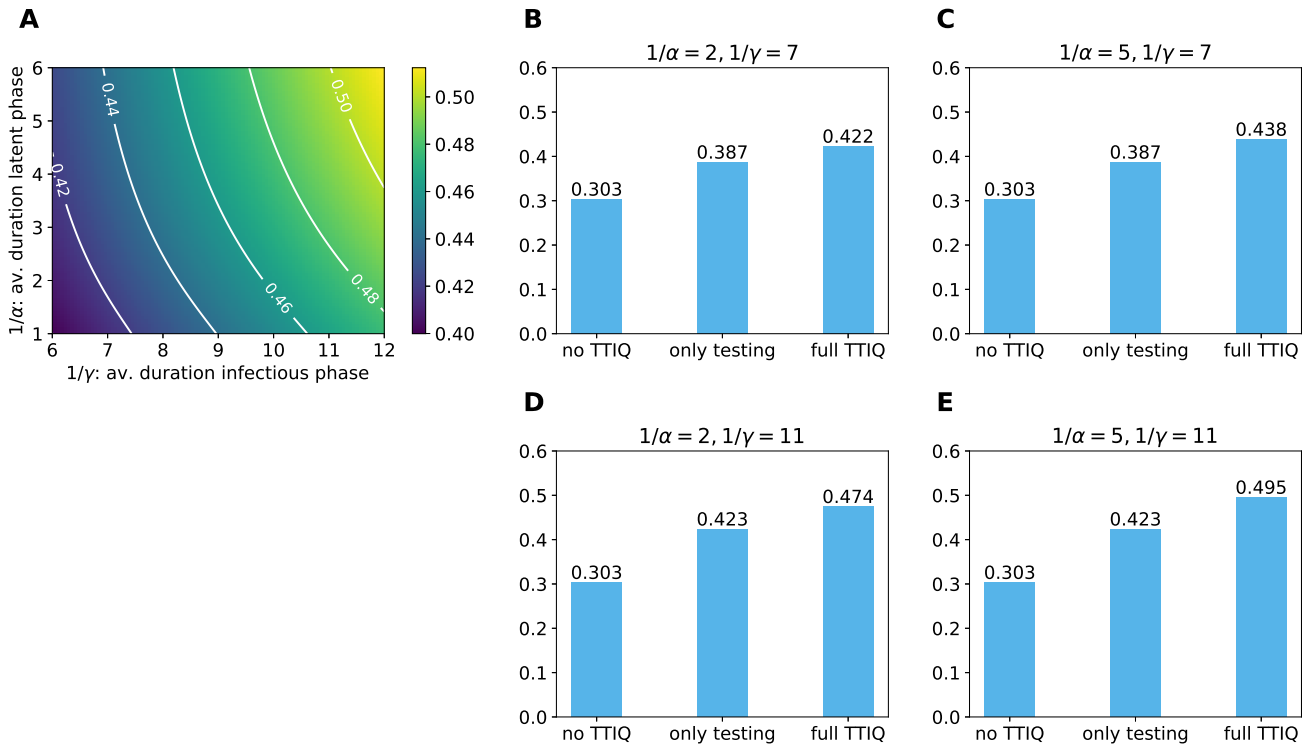


Figure 10: Maximum level ϕ^* of effective contacts that provides stability of the DFE in dependence of **A** the average duration of the latent phase $1/\alpha$ and the average duration of the infectious period $1/\gamma$. In **B-E** different combinations of values for $1/\alpha$ and $1/\gamma$ are considered comparing a scenario without any TTIQ to a scenario where only testing is conducted and a scenario where both testing and contact tracing is carried out.

ϕ^* : maximum allowed level of effective contacts

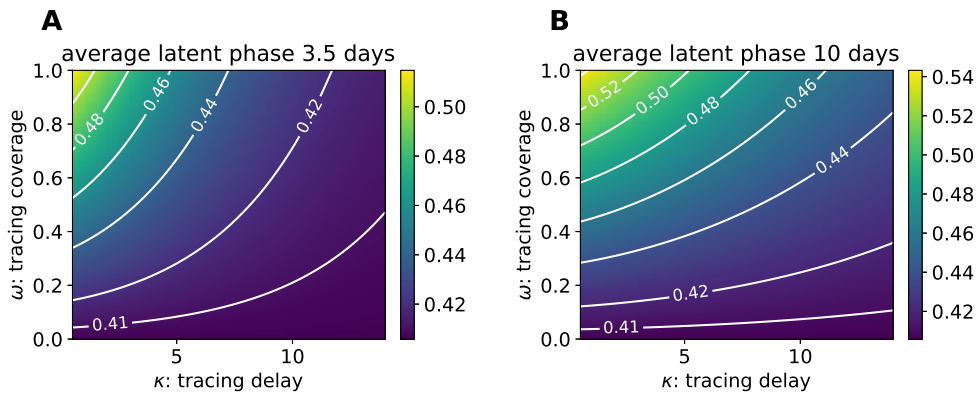


Figure 11: Maximum level ϕ^* of effective contacts that provides stability of the DFE in dependence of the tracing delay κ and the tracing coverage ω assuming an average latent phase of either **A** 3.5 days or **B** 10 days.

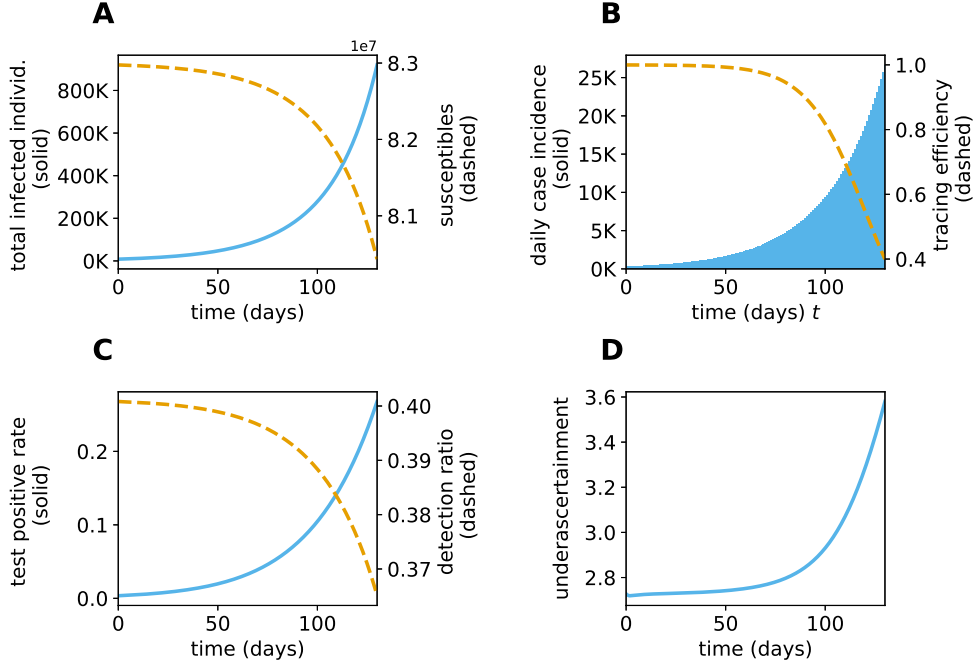


Figure 12: Model outcomes simulating an outbreak starting from low case numbers using baseline parameter values as in Table 2 and a reduction of effective contacts corresponding to $\phi = 0.6$.

low daily incidence of confirmed cases and disease spread is moderately suppressed by contact restrictions. For simplicity, and recognizing that transmission rates and TTIQ effort change much more dynamically in reality, all parameters in this scenario are held constant throughout the simulated period with values as in the baseline setting. In the considered scenario the DFE is unstable leading to an increase in the total number of infected individuals (Figure 12A) and daily new confirmed cases (Figure 12B) over time. As more infectious individuals arise in the population the test positive rate increases (Figure 12C)¹⁶. The finite testing capacity (see equation (3)) leads to a decreasing detection ratio

$$\frac{\eta U_1(t)}{\gamma_1 + \eta U_1(t)} + \frac{\gamma_1}{\gamma_1 + \eta U_1(t)} \frac{\eta U_2(t)}{\gamma_2 + \eta U_2(t)}.$$

The nevertheless increasing number of confirmed cases leads to an increase in reported contacts which gradually diminishes the tracing efficiency (Figure 12B)

$$\varepsilon(t) = \frac{\Omega}{(c_{\text{pot}}(t)^2 + \Omega^2)^{1/2}}.$$

All in all these effects lead to a steep increase in the under-ascertainment of active infectious individuals

$$\frac{U_1(t) + U_2(t) + Q_{U_1}(t) + Q_{U_2}(t) + I_1(t) + I_2(t)}{Q_{U_1}(t) + Q_{U_2}(t) + I_1(t) + I_2(t)}$$

as prevalence rises (Figure 12D).

This loss of control implies a self-accelerating disease spread that gets harder to control the longer it remains uncontrolled. This is reflected in the maximum level $\bar{\phi}$ of effective contacts that achieves a timely stagnation in the incidence of infected individuals. We calculated $\bar{\phi}$ at multiple points in time t^* by simulating an intervention

¹⁶The observed test positive rate appears to be quite high. In reality the relative frequencies σ_X of testing might be state-dependent. In particular, at states of high prevalence all individuals might seek more testing which would lead to higher utilization of test capacity by uninfected individuals and could explain a slower increase in the positive rate.

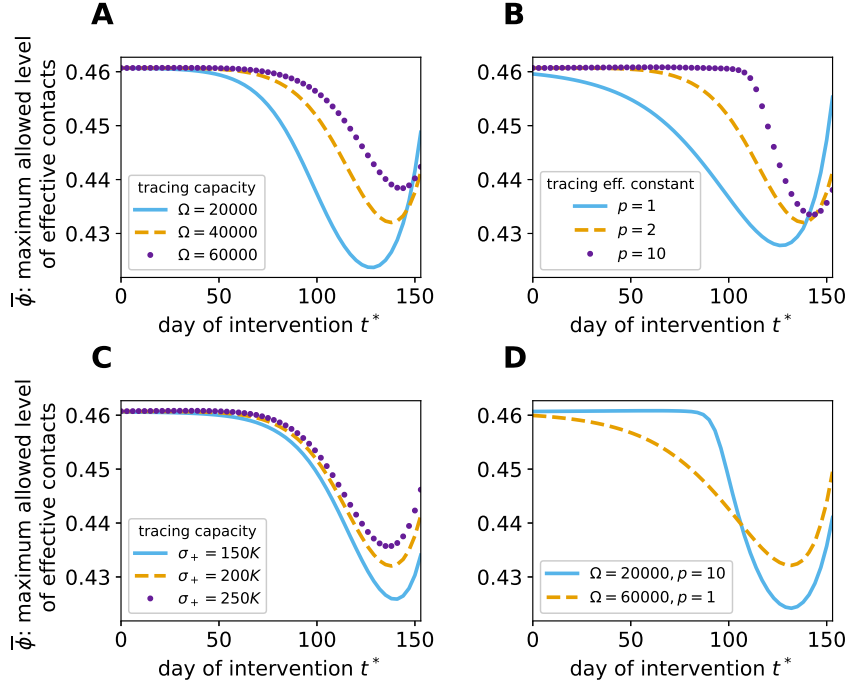


Figure 13: The maximum level $\bar{\phi}$ of effective contacts that achieves a stagnation in the incidence of infected individuals plotted against the timing of intervention t^* calculated along the epidemic outbreak considered in Figure 12 for different values of **A** the tracing capacity Ω , **B** the tracing efficiency constant p , **C** the testing capacity σ_+ and **D** comparing a scenario with high tracing capacity Ω and low tracing efficiency constant p to a scenario with low Ω and large p .

that immediately decreases ϕ , that is

$$\phi(t) = \begin{cases} 0.6, & t < t^* \\ \phi_1, & t \geq t^* \end{cases}$$

and scanned for the maximal value of ϕ_1 that achieves no further increase in the incidence after two weeks post intervention for the rest of the additionally simulated period (+42 days). The result is shown by the dashed line in Figure 13A. Due to the loss of TTIQ effectiveness, later intervention timing t^* requires a stricter reduction of effective contacts (lower $\bar{\phi}$) in order to prevent a further increase in the incidence of infected individuals. However, at some point the effect of population-level immunization (or depletion of susceptibles) counterbalances the effect of a decreasing TTIQ effectiveness and $\bar{\phi}$ starts increasing as t^* becomes larger¹⁷. Models that do not include limited capacities would predict this increase in $\bar{\phi}$ already for early intervention time points t^* .

Impact of capacity parameters

We investigated the impact of TTIQ capacities on the temporal evolution of $\bar{\phi}$ by simulating the epidemic outbreak considered in Figure 12 for multiple values of the tracing capacity Ω , the tracing efficiency constant p (reflecting the efficiency in allocating tracing capacity), and on the testing capacity σ_+ . All three, larger tracing capacity Ω , larger testing capacity σ_+ and larger tracing efficiency constant p (higher efficiency in allocating tracing capacity) increase the minimal value of $\bar{\phi}$ along the outbreak and delay its decrease with respect to t^* (Figure 13A-C). However, for larger p the decrease in $\bar{\phi}$ happens more abruptly. In particular, a TTIQ system with relatively low tracing capacity but with efficient allocation of this capacity (large p) manages to maintain a high tracing efficiency for a longer phase of the outbreak than a TTIQ system with high tracing capacity but inefficient allocation of this capacity (small p). This is only true until a certain prevalence is reached. The system with low absolute tracing

¹⁷Notice that this ease of control comes at the cost of widespread infestation.

$\bar{\phi}$: maximum allowed level of effective contacts

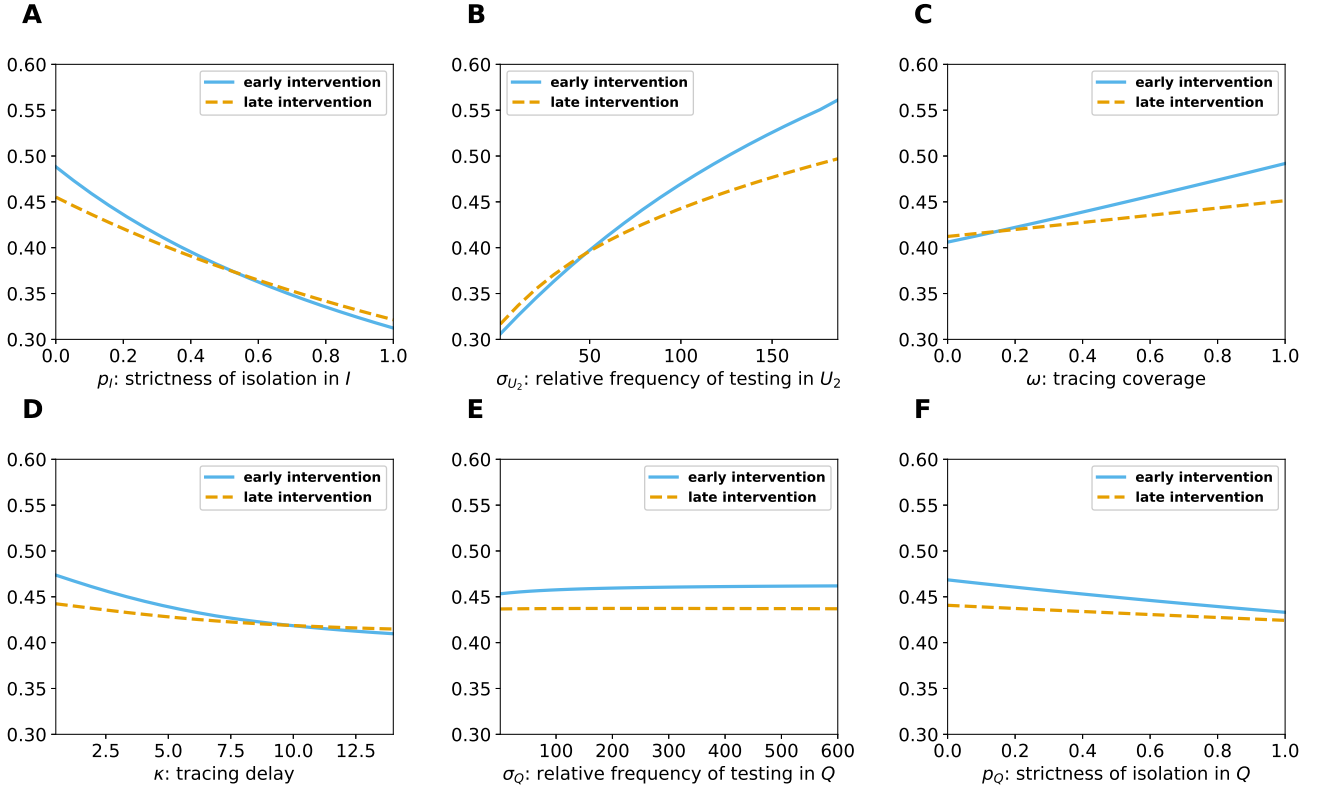


Figure 14: Sensitivity of the maximum level $\bar{\phi}$ of effective contacts that achieves a stagnation in the incidence of infected individuals with respect to variations in single TTIQ parameters at an early intervention time point corresponding to a daily case incidence of approximately 1 500 (solid lines) and at a late intervention time point corresponding to a daily case incidence of approximately 20 000 (dashed lines).

capacity experiences the drop in $\bar{\phi}$ in a shorter time frame and quite abruptly higher levels of population wide contact reductions are needed to regain control over disease spread (Figure 13D).

Implications for intervention strategies

The decrease in TTIQ effectiveness along an epidemic wave implies that the success of intervention strategies is state-dependent. To see how this affects interventions based on changes in TTIQ parameters we considered the outbreak investigated before (see Figure 12) and simulated an intervention taking place either early at a daily case incidence of approximately 1 500 ($t^* = 47$) or late at a daily case incidence of approximately 20 000 ($t^* = 123$). At the start of the intervention we varied TTIQ parameters in ranges as in Table 3 and additionally scanned for the associated maximum level $\bar{\phi}$ of effective contacts that prevents a further increase in the incidence of infected individuals (Figure 14). While the curves corresponding to the early intervention unsurprisingly resemble those in Figure 6, the curves corresponding to the late intervention scenario are shifted. For optimistic TTIQ parameter values, the curves are shifted downwards, reflecting the decreased tracing efficiency and per capita testing rates. Conversely, for suboptimal TTIQ parameter sets, $\bar{\phi}$ is larger in the late intervention scenario due to the already greater depletion of susceptibles. In these cases, the beneficial effect of higher immunization outweighs the detrimental effect of lower TTIQ effectiveness, since TTIQ does not contribute much in the first place. For all TTIQ parameters, the curve corresponding to the late intervention is notably flatter, demonstrating less impact on $\bar{\phi}$ and decreased importance of these parameters for disease control. This concerns, especially, the contact tracing parameters ($\omega, \kappa, \sigma_Q, p_Q$).

The above observations have important implications for the outcome of intervention strategies. To demonstrate

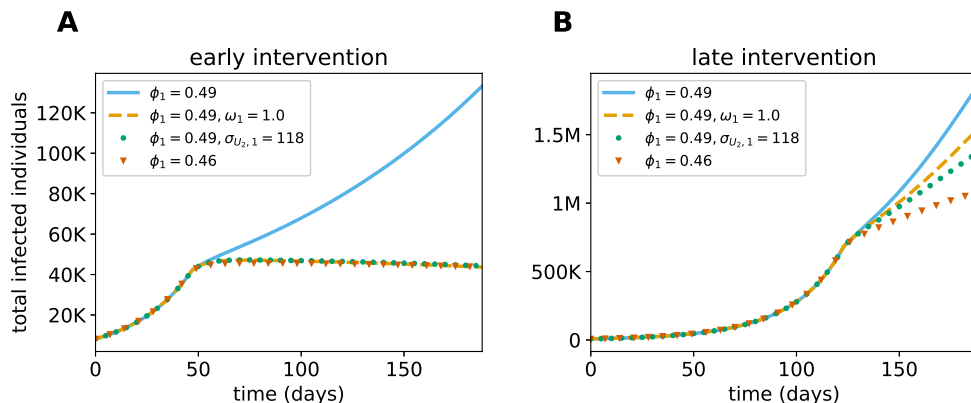


Figure 15: Number of infected individuals (both detected and undetected) simulating the baseline outbreak scenario from Figure 12. Here an intervention takes place either **A** early at a daily case incidence of approximately 1 500 ($t^* = 47$) or **B** late at a daily case incidence of approximately 20 000 ($t^* = 123$). At the time of intervention the level of effective contacts is changed from its baseline value to ϕ_1 . Additionally, in some considered scenarios, the tracing coverage is improved to ω_1 or the relative frequency of testing undetected infectious individuals to $\sigma_{U_2,1}$. These parameter changes are noted in the figure legends. If a specific parameter is not mentioned in the legend, then it is not changed at the time of intervention.

that we report here simulated scenarios where at the day of intervention a stricter reduction of effective contacts (smaller ϕ) is applied and, additionally, for some considered scenarios different TTIQ parameters are improved¹⁸. As before we assumed that the interventions have an immediate effect on the parameters of the system. As a benchmark scenario we assumed that the intervention (applied either early or late as above) leads to a reduction in effective contacts from $\phi = 0.6$ to $\phi_1 = 0.49$. When accompanied with no additional improvements of TTIQ, disease spread is controlled in neither the early nor the late intervention scenario (see solid lines in Figure 15). Additionally increasing the tracing coverage from $\omega = 0.65$ to $\omega_1 = 1$ (e.g., by successfully motivating individuals to keep a contact diary or by improving the close contact definition), improving the relative frequency of testing undetected individuals from $\sigma_{U_2} = 93$ to $\sigma_{U_2,1} = 118$ or implementing a stricter reduction of effective contacts corresponding to $\phi_1 = 0.46$ show a similar response in case of low prevalence and timely lead to a slow decrease in the number of infected individuals (Figure 15A). However, the three enhanced interventions show different responses in the late intervention scenario with high prevalence. Improving the tracing coverage proves to be ineffective (see dashed line Figure 15B), and the improvement in testing does not perform significantly better (see dotted line in Figure 15B). Since this measure is not itself constrained by limited capacities, the stricter reduction of effective contacts performs best and significantly slows down disease spread (see triangles in Figure 15B). All three strategies fail to stop the increase in the number of infected individuals.

4 Discussion

We have presented a mathematical model that allows to assess the impact of TTIQ interventions for infectious disease control. Our approach is based on differential equations and incorporates several of the challenges TTIQ faces. To account for limited testing capacity, we introduce state-dependent testing rates that are based on the mechanistic derivation in [38]. These lead to a reasonably high detection rate of infectious cases at low prevalence that smoothly decreases when prevalence rises. We model contact tracing as a consequence of successful index case identification. Similar to the approach in [28], quarantine of contacts follows index case identification with a constant tracing delay. In contrast to [28], we do not consider a sharp prevalence threshold above which the tracing efficiency is affected by disease spread. Based on a mechanistic relationship between the theoretical yield of detected infections per index case and the curtailment of this yield by the emerging burden on PHA, our

¹⁸We explain how changes in the tracing coverage together with changes in transmission rates are modeled in Appendix B.

model rather describes a smoothly decreasing tracing efficiency as disease prevalence rises. Additionally, as in a previously proposed differential equation model of contact tracing [31], we consider a presymptomatic and highly infectious phase at the beginning of the infectious period.

As a working example representative of a (re-)emerging disease for which pharmaceutical interventions are not yet available, we applied our model to study the effectiveness of TTIQ in the context of the spread of COVID-19 in Germany during the second wave in late summer and fall of 2020. Under these conditions, in particular original strain of SARS-CoV-2, no vaccine, no rapid antigen tests, and low seroprevalence, our model results suggest that, as long as disease prevalence is moderate, TTIQ allows to control disease spread if the reproduction number is reduced to a value below 1.52 by other NPIs alone. Specifically, assuming a basic reproduction number of 3.3, TTIQ allows for approximately 52% more effective contacts within the population. Nevertheless, even with TTIQ as described here a reduction to approximately 46% of the pre-COVID-19 effective contact rate would be needed to prevent an epidemic outbreak. This is in line with previous modeling studies suggesting that additional NPIs or pharmaceutical interventions are required to control disease spread under realistic assumptions on imperfect TTIQ [4, 13, 16, 19, 20, 22–24, 28, 29, 37].

By means of a sensitivity analysis we identified the TTIQ parameters most influential to the effectiveness of TTIQ. Our approach underlines previous findings of the major importance of compliance with isolation [13, 17, 19] and the rate of index case identification [13, 16, 18–20, 23, 27]. The significance of these parameters reflects simple causal relationships between the mechanisms described by the TTIQ parameters. It is irrelevant how many index cases are found by testing and how many contacts are traced when none of them effectively reduces their contacts. Similarly, by definition contacts can only be traced and quarantined upon prior identification of index cases. This renders the success of testing a key factor for the effectiveness of TTIQ. Consistent with the studies in [27, 29, 32], we observed synergistic effects when varying TTIQ parameters simultaneously which highlights the benefit of combining strategies rather than concentrating on, e.g., testing exclusively. We do not observe significant differences between the importance of the tracing coverage and the tracing delay. Both low coverage and long delay render contact tracing completely ineffective.

To go beyond our consideration of COVID-19 and to further assess the effect of uncertainty in our baseline parameter setting we considered variations in parameters describing disease characteristics. The already described importance of the index case identification rate demonstrates the significant impact of asymptomatic or paucisymptomatic courses of the disease on a symptom-based testing strategy (see also [16, 20, 22, 24, 27, 35]). Similarly, we find a significantly different TTIQ effectiveness when varying the amount of presymptomatic infections (in line with [12, 20, 35]). Furthermore, we considered the time scale of disease spread and varied the average duration of the latent phase and of the infectious period. Our results demonstrate that a prolonged latent phase solely affects contact tracing, but not testing, and decreases the sensitivity of TTIQ effectiveness to (low values of) the tracing delay. In contrast, a longer infectious period improves benefits of both the testing and the contact tracing process. Overall, our results underline that COVID-19 combines several characteristics adverse to TTIQ (asymptomatic and presymptomatic transmissions, short latency and infectious period, airborne transmission resulting in imperfect tracing coverage) that explain its rather low effectiveness observed in our baseline setting.

When disease control is insufficient and an outbreak takes place, limited TTIQ capacities lead to a self-acceleration of disease spread [28, 29, 31, 37]. In our model, this effect takes place smoothly along an epidemic wave until it is countered by sufficiently wide spread immunization. We show how the timing and intensity of the self-accelerating effect depend on the capacity parameters. It is weaker for higher capacities and a more efficient allocation of contact tracing expressed by larger tracing efficiency constant p . Moreover, a larger p extends the period of almost perfect tracing efficiency and leads to a more abrupt decrease of tracing efficiency. The limit $p \rightarrow \infty$ offers a transition between the description of tracing capacity in our model and previous models that assume a sharp prevalence threshold for the decrease in tracing efficiency [28, 29, 37]. The self-accelerating effect observed in our working example appears to be only moderate. It may be more or less pronounced depending on assumptions on the model structure and parameters (see, e.g., [28]). Either way the detrimental effect of limited capacity in our simulations – though less pronounced than under alternative modeling assumptions – is far from negligible. In particular, the transient acceleration of disease spread can have irreversible effects [37]. Moreover, our study suggests that TTIQ can be substantially more effective for infectious diseases with different epidemiological characteristics. It should be noticed, that in these cases exhausted capacities have a stronger effect on disease spread and the benefit of maintaining low prevalence is further amplified.

Additionally, our results show that at states of high prevalence TTIQ effectiveness is less sensitive to changes in parameters. In consequence, this implies that not only stricter measures are needed to control disease spread

but interventions based on improvements in TTIQ parameters become less effective. In such situations, greater reduction of transmission rates by means of stricter social or hygiene measures might be the only feasible NPI to effectively stop case numbers from rising. This demonstrates that a careful evaluation of the contemporary load on TTIQ capacities is needed to predict the effect of different intervention strategies.

There are several limitations to our model that offer routes for further research. We concentrated on first-order manual forward tracing. Other modeling studies consider the effect of recursive tracing [14, 16, 21, 25], backward tracing [15, 25, 26] and digital contact tracing [4, 16, 23, 24]. Under favorable conditions¹⁹ these processes can add significantly to the effectiveness of TTIQ which should be considered when interpreting our results. Moreover, in reality, a relevant proportion of contacts of confirmed cases is likely to be informed about their potential transmission by the index case before PHA reach out to the contact. This can lead to earlier quarantine of contacts and render parts of contact tracing independent of PHA capacities. Similarly, individuals might reduce their contacts due to an increase in reported cases or because they start to show signs of being infected. The latter would lead to some infectious individuals starting to isolate before their infection is confirmed by testing. These and other behavioral factors are so far not considered in our model. Moreover, we only consider quarantine for contacts that got indeed infected by one of the identified index cases. It should be noticed that, quarantine of the remaining contacts (those that had contact but were not infected), which is for example considered in [16, 31, 32, 34], might have a noticeable effect on disease dynamics if sufficiently many susceptibles are quarantined or additional infected individuals are found²⁰. In addition, the consideration of quarantine of all contacts (infected and uninfected) would allow to assess the socioeconomic damage induced by contact tracing and to address TTIQ strategies that reduce quarantine costs (see for example [17, 24, 31, 42]). Furthermore, our approach considers the populations in the different compartments in our model as homogeneous. At the cost of an extended parameter space many additional factors that differentiate individuals could be considered, such as age, space, overdispersion and disease severity. For instance, the significant benefit of increasing the relative frequency σ_{U_2} of testing undetected infectious individuals when compared to susceptibles shown in Figure 6C should be seen as harder to realize the larger σ_{U_2} becomes. Every increase of σ_{U_2} deviates the typical distribution of individuals in U_2 more and more towards paucisymptomatic individuals. This makes the average individual in U_2 less amenable to symptom-based testing and a further increase of σ_{U_2} more difficult to achieve. Moreover, it should be noticed that we considered a constant tracing delay. More realistically, there is a certain variability in the tracing delay (see for example [25]) and PHA have to find the right balance between tracing coverage and speed as the workload increases during an epidemic wave. Furthermore, our approach assumes homogeneous mixing. However, the effect of contact tracing is dependent on the contact network underlying the considered population. Previous modeling studies found that, for instance, clustering benefits contact tracing [43, 44] and that mixing patterns can affect the efficacy of contact tracing [14]. Furthermore, although our model splits the infectious phase into a presymptomatic and symptomatic compartment, a more realistic infectivity profile and course of symptoms could be considered using an age of infection approach [4, 16, 25, 26, 35–37]. These approaches are highly involved and lead to the formulation of partial differential and integro-differential equations. This would offer a natural environment to overcome many approximations that we applied in the derivation of the contact tracing terms. It would be desirable to build a mathematical framework that incorporates the capacity problem as detailed as in our work in an age of infection framework. An agent-based framework [12, 13, 16, 17] would allow to include even more complexity and to consider various of the factors outlined above. A comparison to such complex formulations of contact tracing could be used to investigate the justification of a numerically inexpensive but approximate model as leveraged in the present work.

In conclusion, our work extends the current literature on mean-field models of TTIQ. Our detailed mechanistic model accounts for challenges to TTIQ posed by disease characteristics and inherent limitations such as a tracing delay, imperfect compliance with isolation, and limited testing and tracing resources. Our simulation results, using the spread of COVID-19 as an example, show how these factors can limit the effectiveness of TTIQ as a strategy for disease control. A strength of our approach is that we disentangle the individual contribution of the separate processes of finding index cases and then tracing their contacts to disease control. Our model is flexible enough to be adapted and applied to evaluate the effectiveness of TTIQ to control other infectious disease.

¹⁹For example digital contact tracing depends on widespread adoption and as argued in [41] the effectiveness of backward tracing depends on disease characteristics and can suffer from recall problems.

²⁰This becomes relevant only at a high prevalence.

Acknowledgments

MVB and JH were supported by the LOEWE focus CMMS.

Conflict of interest

We have no conflict of interest to declare.

Code availability

The code necessary to reproduce the results presented in this work is available under: <https://github.com/julehe/TTIQ>.

References

- [1] J. Baj, H. Karakuła-Juchnowicz, G. Teresiński, G. Buszewicz, M. Ciesielka, E. Sitarz, et al., COVID-19: Specific and non-specific clinical manifestations and symptoms: The current state of knowledge, *Journal of Clinical Medicine*, **9** (2020), 1753. <https://doi.org/10.3390/jcm9061753>
- [2] R. da Rosa Mesquita, L. C. F. S. Junior, F. M. S. Santana, T. F. de Oliveira, R. C. Alcântara, G. M. Arnozo, et al., Clinical manifestations of COVID-19 in the general population: systematic review, *Wiener klinische Wochenschrift*, **133** (2020), 377–382. <https://doi.org/10.1007/s00508-020-01760-4>
- [3] *Robert Koch Institute*, Epidemiologischer Steckbrief zu SARS-CoV-2 und COVID-19, Last accessed on 07/07/2022. Available from: https://www.rki.de/DE/Content/InfAZ/N/Neuartiges_Coronavirus/Steckbrief.html.
- [4] L. Ferretti, C. Wymant, M. Kendall, L. Zhao, A. Nurtay, L. Abeler-Dörner, et al., Quantifying SARS-CoV-2 transmission suggests epidemic control with digital contact tracing, *Science*, **368** (2020), eabb6936. <https://doi.org/10.1126/science.abb6936>
- [5] T. Ganyani, C. Kremer, D. Chen, A. Torneri, C. Faes, J. Wallinga, et al., Estimating the generation interval for coronavirus disease (COVID-19) based on symptom onset data, March 2020, *Eurosurveillance*, **25** (2020), 2000257. <https://doi.org/10.2807/1560-7917.es.2020.25.17.2000257>
- [6] X. He, E. H. Y. Lau, P. Wu, X. Deng, J. Wang, X. Hao, et al., Temporal dynamics in viral shedding and transmissibility of COVID-19, *Nature Medicine*, **26** (2020), 672–675. <https://doi.org/10.1038/s41591-020-0869-5>
- [7] J. Bullard, K. Dust, D. Funk, J. E. Strong, D. Alexander, L. Garnett, et al., Predicting Infectious Severe Acute Respiratory Syndrome Coronavirus 2 From Diagnostic Samples, *Clinical Infectious Diseases*, **71** (2020), 2663–2666. <https://doi.org/10.1093/cid/ciaa638>
- [8] R. Li, S. Pei, B. Chen, Y. Song, T. Zhang, W. Yang, et al., Substantial undocumented infection facilitates the rapid dissemination of novel coronavirus (SARS-CoV-2), *Science*, **368** (2020), 489–493. <https://doi.org/10.1126/science.abb3221>

- [9] A. Singanayagam, M. Patel, A. Charlett, J. L. Bernal, V. Saliba, J. Ellis, et al., Duration of infectiousness and correlation with RT-PCR cycle threshold values in cases of COVID-19, England, January to May 2020, *Eurosurveillance*, **25** (2020), 2001483. <https://doi.org/10.2807/1560-7917.es.2020.25.32.2001483>
- [10] R. Wölfel, V. M. Corman, W. Guggemos, M. Seilmaier, S. Zange, M. A. Müller, et al., Virological assessment of hospitalized patients with COVID-2019, *Nature*, **581** (2020), 465–469. <https://doi.org/10.1038/s41586-020-2196-x>
- [11] J. Müller, M. Kretzschmar, Contact tracing – Old models and new challenges, *Infectious Disease Modelling*, **6** (2021), 222–231. <https://doi.org/10.1016/j.idm.2020.12.005>
- [12] K. F. Jarvis, J. B. Kelley, Temporal dynamics of viral load and false negative rate influence the levels of testing necessary to combat COVID-19 spread, *Scientific Reports*, **11** (2021), 9221. <https://doi.org/10.1038/s41598-021-88498-9>
- [13] C. C. Kerr, D. Mistry, R. M. Stuart, K. Rosenfeld, G. R. Hart, R. C. Núñez, et al., Controlling COVID-19 via test-trace-quarantine, *Nature Communications*, **12** (2021), 2993. <https://doi.org/10.1038/s41467-021-23276-9>
- [14] I. Z. Kiss, D. M. Green, R. R. Kao, The effect of network mixing patterns on epidemic dynamics and the efficacy of disease contact tracing, *Journal of The Royal Society Interface*, **5** (2007), 791–799. <https://doi.org/10.1098/rsif.2007.1272>
- [15] S. Kojaku, L. Hébert-Dufresne, E. Mones, S. Lehmann, Y.-Y. Ahn, The effectiveness of backward contact tracing in networks, *Nature Physics*, **17** (2021), 652–658. <https://doi.org/10.1038/s41567-021-01187-2>
- [16] T. R. Pollmann, S. Schönert, J. Müller, J. Pollmann, E. Resconi, C. Wiesinger, et al., The impact of digital contact tracing on the SARS-CoV-2 pandemic—a comprehensive modelling study, *EPJ Data Science*, **10** (2021), 37. <https://doi.org/10.1140/epjds/s13688-021-00290-x>
- [17] B. J. Quilty, S. Clifford, J. Hellewell, T. W. Russell, A. J. Kucharski, S. Flasche, et al., Quarantine and testing strategies in contact tracing for SARS-CoV-2: a modelling study, *The Lancet Public Health*, **6** (2021), e175–e183. [https://doi.org/10.1016/S2468-2667\(20\)30308-X](https://doi.org/10.1016/S2468-2667(20)30308-X)
- [18] P. Ashcroft, S. Lehtinen, S. Bonhoeffer, Test-trace-isolate-quarantine (TTIQ) intervention strategies after symptomatic COVID-19 case identification, *PLOS ONE*, **17** (2022), e0263597. <https://doi.org/10.1371/journal.pone.0263597>
- [19] E. L. Davis, T. C. D. Lucas, A. Borlase, T. M. Pollington, S. Abbott, D. Ayabina, et al., Contact tracing is an imperfect tool for controlling COVID-19 transmission and relies on population adherence, *Nature communications*, **12** (2021), 5412. <https://doi.org/10.1038/s41467-021-25531-5>
- [20] J. Hellewell, S. Abbott, A. Gimma, N. I. Bosse, C. I. Jarvis, T. W. Russell, et al., Feasibility of controlling COVID-19 outbreaks by isolation of cases and contacts, *The Lancet Global Health*, **8** (2020), e488–e496. [https://doi.org/10.1016/S2214-109X\(20\)30074-7](https://doi.org/10.1016/S2214-109X(20)30074-7)
- [21] D. Klinkenberg, C. Fraser, H. Heesterbeek, The Effectiveness of Contact Tracing in Emerging Epidemics, *PLoS ONE*, **1** (2006), e12. <https://doi.org/10.1371/journal.pone.0000012>

- [22] M. E. Kretzschmar, G. Rozhnova, M. van Boven, Isolation and Contact Tracing Can Tip the Scale to Containment of COVID-19 in Populations With Social Distancing, *Frontiers in Physics*, **8** (2021), 622485. <https://doi.org/10.3389/fphy.2020.622485>
- [23] M. E. Kretzschmar, G. Rozhnova, M. C. J. Bootsma, M. van Boven, J. H. H. M. van de Wiggert, M. J. M. Bonten, Impact of delays on effectiveness of contact tracing strategies for COVID-19: a modelling study, *The Lancet Public Health*, **5** (2020), e452–e459. [https://doi.org/10.1016/S2468-2667\(20\)30157-2](https://doi.org/10.1016/S2468-2667(20)30157-2)
- [24] A. J. Kucharski, P. Klepac, A. J. K. Conlan, S. M. Kissler, M. L. Tang, H. Fry, et al., Effectiveness of isolation, testing, contact tracing, and physical distancing on reducing transmission of SARS-CoV-2 in different settings: a mathematical modelling study, *The Lancet Infectious Diseases*, **20** (2020), 1151–1160. [https://doi.org/10.1016/S1473-3099\(20\)30457-6](https://doi.org/10.1016/S1473-3099(20)30457-6)
- [25] J. Müller, B. Koopmann, The effect of delay on contact tracing, *Mathematical Biosciences*, **282** (2016), 204–214. <https://doi.org/10.1016/j.mbs.2016.10.010>
- [26] J. Müller, M. Kretzschmar, K. Dietz, Contact tracing in stochastic and deterministic epidemic models, *Mathematical Biosciences*, **164** (2000), 39–64. [https://doi.org/10.1016/s0025-5564\(99\)00061-9](https://doi.org/10.1016/s0025-5564(99)00061-9)
- [27] C. Browne, H. Gulbudak, G. Webb, Modeling contact tracing in outbreaks with application to Ebola, *Journal of Theoretical Biology*, **384** (2015), 33–49. <https://doi.org/10.1016/j.jtbi.2015.08.004>
- [28] S. Contreras, J. Dehning, S. B. Mohr, S. Bauer, F. P. Spitzner, V. Priesemann, Low case numbers enable long-term stable pandemic control without lockdowns, *Science advances*, **7** (2021), eabg2243. <https://doi.org/10.1126/sciadv.abg2243>
- [29] S. Contreras, J. Dehning, M. Loidolt, J. Zierenberg, F. P. Spitzner, J. H. Urrea-Quintero, et al., The challenges of containing SARS-CoV-2 via test-trace-and-isolate, *Nature Communications*, **12** (2021), 378. <https://doi.org/10.1038/s41467-020-20699-8>
- [30] G. Giordano, F. Blanchini, R. Bruno, P. Colaneri, A. D. Filippo, A. D. Matteo, et al., Modelling the COVID-19 epidemic and implementation of population-wide interventions in Italy, *Nature Medicine*, **26** (2020), 855–860. <https://doi.org/10.1038/s41591-020-0883-7>
- [31] D. Lunz, G. Batt, J. Ruess, To quarantine, or not to quarantine: A theoretical framework for disease control via contact tracing, *Epidemics*, **34** (2021), 100428. <https://doi.org/10.1016/j.epidem.2020.100428>
- [32] S. Sturniolo, W. Waites, T. Colbourn, D. Manheim, J. Panovska-Griffiths, Testing, tracing and isolation in compartmental models, *PLoS Computational Biology*, **17** (2021), e1008633. <https://doi.org/10.1371/journal.pcbi.1008633>
- [33] B. Tang, F. Scarabel, N. L. Bragazzi, Z. McCarthy, M. Glazer, Y. Xiao, et al., De-Escalation by Reversing the Escalation with a Stronger Synergistic Package of Contact Tracing, Quarantine, Isolation and Personal Protection: Feasibility of Preventing a COVID-19 Rebound in Ontario, Canada, as a Case Study, *Biology*, **9** (2020), 100. <https://doi.org/10.3390/biology9050100>
- [34] G. Webb, C. Brown, X. Huo, O. Seydi, M. Seydi, P. Magal, A model of the 2014 ebola epidemic in west africa with contact tracing, *PLoS Currents*, **7** (2015). <https://doi.org/10.1371/currents.outbreaks.846b2a31ef37018b7d1126a9c8adf22a>

- [35] C. Fraser, S. Riley, R. M. Anderson, N. M. Ferguson, Factors that make an infectious disease outbreak controllable, *Proceedings of the National Academy of Sciences*, **101** (2004), 6146–6151. <https://doi.org/10.1073/pnas.0307506101>
- [36] X. Huo, Modeling of contact tracing in epidemic populations structured by disease age, *Discrete & Continuous Dynamical Systems - B*, **20** (2015), 1685–1713. <http://dx.doi.org/10.3934/dcdsb.2015.20.1685>
- [37] F. Scarabel, L. Pellis, N. H. Ogden, J. Wu, A renewal equation model to assess roles and limitations of contact tracing for disease outbreak control, *Royal Society Open Science*, **8** (2021), 202091. <https://doi.org/10.1098/rsos.202091>
- [38] M. V. Barbarossa, J. Fuhrmann, Compliance with NPIs and possible deleterious effects on mitigation of an epidemic outbreak, *Infectious Disease Modelling*, **6** (2021), 859–874. <https://doi.org/10.1016/j.idm.2021.06.001>
- [39] F. Brauer, C. Castillo-Chavez, Z. Feng, *Mathematical Models in Epidemiology*, Springer New York, 2019. <https://doi.org/10.1007/978-1-4939-9828-9>
- [40] S. Marino, I. B. Hogue, C. J. Ray, D. E. Kirschner, A methodology for performing global uncertainty and sensitivity analysis in systems biology, *Journal of Theoretical Biology*, **254** (2008), 178–196. <https://doi.org/10.1016/j.jtbi.2008.04.011>
- [41] J. Müller, M. Kretzschmar, Forward thinking on backward tracing, *Nature Physics*, **17** (2021), 555–556. <https://doi.org/10.1038/s41567-021-01188-1>
- [42] P. Ashcroft, S. Lehtinen, D. C. Angst, N. Low, S. Bonhoeffer, Quantifying the impact of quarantine duration on COVID-19 transmission, *eLife*, **10** (2021), e63704. <https://doi.org/10.7554/eLife.63704>
- [43] K. T. D. Eames, M. J. Keeling, Contact tracing and disease control, *Proceedings of the Royal Society of London. Series B: Biological Sciences*, **270** (2003), 2565–2571. <https://doi.org/10.1098/rspb.2003.2554>
- [44] T. House, M. J. Keeling, The impact of contact tracing in clustered populations, *PLoS Computational Biology*, **6** (2010), e1000721. <https://doi.org/10.1371/journal.pcbi.1000721>
- [45] S. A. Lauer, K. H. Grantz, Q. Bi, F. K. Jones, Q. Zheng, H. R. Meredith, et al., The Incubation Period of Coronavirus Disease 2019 (COVID-19) From Publicly Reported Confirmed Cases: Estimation and Application, *Annals of Internal Medicine*, **172** (2020), 577–582. <https://doi.org/10.7326/m20-0504>
- [46] Q. Li, X. Guan, P. Wu, X. Wang, L. Zhou, Y. Tong, et al., Early Transmission Dynamics in Wuhan, China, of Novel Coronavirus-Infected Pneumonia, *New England Journal of Medicine*, **382** (2020), 1199–1207. <https://doi.org/10.1056/nejmoa2001316>
- [47] Y. Alimohamadi, M. Taghdir, M. Sepandi, Estimate of the Basic Reproduction Number for COVID-19: A Systematic Review and Meta-analysis, *Journal of Preventive Medicine and Public Health*, **53** (2020), 151–157. <https://doi.org/10.3961/jpmph.20.076>
- [48] M. A. Billah, M. M. Miah, M. N. Khan, Reproductive number of coronavirus: A systematic review and meta-analysis based on global level evidence, *PLOS ONE*, **15** (2020), e0242128. <https://doi.org/10.1371/journal.pone.0242128>

- [49] S. Zhao, Q. Lin, J. Ran, S. S. Musa, G. Yang, W. Wang, et al., Preliminary estimation of the basic reproduction number of novel coronavirus (2019-nCoV) in China, from 2019 to 2020: A data-driven analysis in the early phase of the outbreak, *International Journal of Infectious Diseases*, **92** (2020), 214–217. <https://doi.org/10.1016/j.ijid.2020.01.050>
- [50] *Robert Koch Institute*, Erfassung der SARS-CoV-2-Testzahlen in Deutschland, Last accessed on 07/07/2022. Available from: https://www.rki.de/DE/Content/InfAZ/N/Neuartiges_Coronavirus/Testzahl.html.
- [51] Y. Kuang, *Delay Differential Equations: With Applications in Population Dynamics*, Academic press, 1993.
- [52] E. Jarlebring, Some numerical methods to compute the eigenvalues of a time-delay system using Matlab, *The delay e-letter*, **2** (2008), 155.
- [53] L. N. Trefethen, *Spectral Methods in MATLAB*, Society for Industrial and Applied Mathematics, 2000.
- [54] C. R. Harris, K. J. Millman, S. J. van der Walt, R. Gommers, P. Virtanen, D. Cournapeau, et al., Array programming with NumPy, *Nature*, **585** (2020), 357–362. <https://doi.org/10.1038/s41586-020-2649-2>
- [55] P. Virtanen, R. Gommers, T. E. Oliphant, M. Haberland, T. Reddy, D. Cournapeau, et al., SciPy 1.0: fundamental algorithms for scientific computing in Python, *Nature Methods*, **17** (2020), 261–272. <https://doi.org/10.1038/s41592-019-0686-2>
- [56] J. D. Hunter, Matplotlib: A 2D Graphics Environment, *Computing in Science & Engineering*, **9** (2007), 90–95. <https://doi.org/10.1109/MCSE.2007.55>
- [57] ddeint Developer, ddeint, Version 0.2 (2019). <https://pypi.org/project/ddeint/>
- [58] R. Vallat, Pingouin: statistics in Python, *Journal of Open Source Software*, **3** (2018), 1026. <https://doi.org/10.21105/joss.01026>

Appendix A Incorporation of a presymptomatic infectious period

In this section we outline the derivation of the terms Tr_E, Tr_{U_1}, Tr_{U_2} describing contact tracing in the model (14) with presymptomatic transmission. To this end, we distinguish between index cases detected while being in their presymptomatic phase U_1 and those being detected while being in their symptomatic phase U_2 . These different types of index cases report on average different numbers of infected contacts, and their contacts spent a different duration in the infected chain at the time of being quarantined.

First, consider an average index case detected by testing at time $t - \kappa$ while being in U_2 (here called U_2 -index case). Following the same reasoning as in Section 2.2, we assume that the PHA choose a tracing window T and ask for close contacts from the tracing interval $J_{t,T}^{U_2} = [t - \kappa - T, t - \kappa]$. The index case’s age of infection $\tau_t^{U_2}$ (by the time of detection $t - \kappa$) is the sum of the time spent in U_1 and the time spent in U_2 ,

$$\tau_t^{U_2} = \tau_{t,U_1}^{U_2} + \tau_{t,U_2}^{U_2}.$$

Depending on the tracing window T , the tracing interval $J_{t,T}^{U_2}$ is composed of three subintervals:

- the (potentially trivial) part of $J_{t,T}^{U_2}$ during which the index case was not yet infectious

$$J_{t,T}^{U_2, \text{minf}} = \begin{cases} \emptyset, & \text{if } T \leq \tau_t^{U_2} \\ [t - \kappa - T, t - \kappa - \tau_t^{U_2}], & \text{if } T > \tau_t^{U_2} \end{cases}$$

- the (potentially trivial) part of $J_{t,T}^{U_2}$ where the index case was infectious and presymptomatic

$$J_{t,T}^{U_2, \text{pre}} = \begin{cases} \emptyset, & \text{if } T \leq \tau_{t,U_2}^{U_2} \\ [t - \kappa - T, t - \kappa - \tau_{t,U_2}^{U_2}], & \text{if } \tau_{t,U_2}^{U_2} < T \leq \tau_t^{U_2} \\ [t - \kappa - \tau_t^{U_2}, t - \kappa - \tau_{t,U_2}^{U_2}], & \text{if } T > \tau_t^{U_2} \end{cases} \quad (18)$$

- the time in $J_{t,T}^{U_2}$ during which the index case was in the symptomatic phase

$$J_{t,T}^{U_2, \text{sym}} = \begin{cases} [t - \kappa - T, t - \kappa], & \text{if } T \leq \tau_{t,U_2}^{U_2} \\ [t - \kappa - \tau_{t,U_2}^{U_2}, t - \kappa], & \text{if } T > \tau_{t,U_2}^{U_2}. \end{cases} \quad (19)$$

In reality, the close contact definition probably leads to different reported close contact rates $\tilde{c}_0, \tilde{c}_1, \tilde{c}_2$ corresponding to $J_{t,T}^{U_2, \text{minf}}, J_{t,T}^{U_2, \text{pre}}, J_{t,T}^{U_2, \text{sym}}$ and different infection probabilities \tilde{p}_1, \tilde{p}_2 corresponding to $J_{t,T}^{U_2, \text{pre}}, J_{t,T}^{U_2, \text{sym}}$. These result in transmission rates observed by contact tracing $\tilde{\beta}_1 := \tilde{p}_1 \tilde{c}_1$ in $J_{t,T}^{U_2, \text{pre}}$ and $\tilde{\beta}_2 := \tilde{p}_2 \tilde{c}_2$ in $J_{t,T}^{U_2, \text{sym}}$. Following our argumentation in Section 2.2, we make the simplifying assumption that $\tilde{c} := \tilde{c}_0 = \tilde{c}_1 = \tilde{c}_2$. Additionally, we set $\tilde{p}_1 = \theta \tilde{p}_2$, where θ is the scaling factor for the transmission rate in the presymptomatic phase. Note that this results in

$$\frac{\tilde{\beta}_1}{\beta_{U_1}} = \frac{\tilde{\beta}_2}{\beta_{U_2}}. \quad (20)$$

Following the approach in Section 2.2, we approximate the rate at which contacts of U_2 -index cases become traceable at time t as

$$c_{\text{pot}}^{U_2}(t) = \left| J_{t,T}^{U_2} \right| \tilde{c} \eta_{U_2}(t - \kappa) U_2(t - \kappa). \quad (21)$$

The rate at which infected contacts of U_2 -index cases become traceable at time t is the sum of those infected while their U_2 -index case was in U_1

$$c_{\text{pot}, U_1}^{\text{inf}, U_2}(t) = \frac{\left| J_{t,T}^{U_2, \text{pre}} \right|}{\left| J_{t,T}^{U_2} \right|} \tilde{p}_1 \frac{S(t - \kappa)}{N} c_{\text{pot}}^{U_2}(t)$$

and those infected while their U_2 -index case was in U_2

$$c_{\text{pot}, U_2}^{\text{inf}, U_2}(t) = \frac{\left| J_{t,T}^{U_2, \text{sym}} \right|}{\left| J_{t,T}^{U_2} \right|} \tilde{p}_2 \frac{S(t - \kappa)}{N} c_{\text{pot}}^{U_2}(t).$$

We approximate the time that contacts, infected while their U_2 -index case was in U_1 , have spent in the infected chain by the time t of being traced as

$$\tilde{r}_{U_1}^{U_2}(t) = \kappa + \frac{1}{2} \left| J_{t,T}^{U_2, \text{pre}} \right| + \left| J_{t,T}^{U_2, \text{sym}} \right|. \quad (22)$$

For those contacts, infected while their U_2 -index case was in U_2 , we approximate this time as

$$\tilde{r}_{U_2}^{U_2}(t) = \kappa + \frac{1}{2} \left| J_{t,T}^{U_2, \text{sym}} \right|. \quad (23)$$

Let us now consider an average index case detected at time $t - \kappa$ while being in U_1 (U_1 -index case). For simplicity, we assume that the same tracing window T as for U_2 -index cases is chosen, thus, the index case is asked to share close contacts from $J_{t,T}^{U_1} = [t - \kappa - T, t - \kappa]$. Denote the time the average U_1 -index has been infectious by the time $t - \kappa$ of being detected by $\tau_t^{U_1}$. Depending on the relationship between T and $\tau_t^{U_1}$, the tracing interval $J_{t,T}^{U_1}$ is composed of two subintervals:

- the potentially trivial part of $J_{t,T}^{U_1}$ during which the index case was not yet infectious

$$J_{t,T}^{U_1, \text{inf}} = \begin{cases} \emptyset, & \text{if } T \leq \tau_t^{U_1} \\ [t - \kappa - T, t - \kappa - \tau_t^{U_1}], & \text{if } T > \tau_t^{U_1} \end{cases}$$

- the time in $J_{t,T}^{U_1}$ during which the index case was infectious and presymptomatic

$$J_{t,T}^{U_1, \text{pre}} = \begin{cases} [t - \kappa - T, t - \kappa], & \text{if } T \leq \tau_t^{U_1} \\ [t - \kappa - \tau_t^{U_1}, t - \kappa], & \text{if } T > \tau_t^{U_1}. \end{cases} \quad (24)$$

We approximate the rate at which contacts of U_1 -index cases become traceable at time t as

$$c_{\text{pot}}^{U_1}(t) = \left| J_{t,T}^{U_1} \right| \tilde{c} \eta_{U_1}(t - \kappa) U_1(t - \kappa). \quad (25)$$

The rate at which infected contacts of U_1 -index cases become traceable at time t is approximated as

$$c_{\text{pot}}^{\text{inf}, U_1}(t) = \frac{\left| J_{t,T}^{U_1, \text{pre}} \right|}{\left| J_{t,T}^{U_1} \right|} \tilde{p}_1 \frac{S(t - \kappa)}{N} c_{\text{pot}}^{U_1}(t).$$

The time such contacts have stayed in the infected chain by the time of being traced t is estimated as

$$\tilde{r}^{U_1}(t) = \kappa + \frac{1}{2} \left| J_{t,T}^{U_1, \text{pre}} \right|. \quad (26)$$

The sum of (21) and (25) gives the total rate at which contacts become traceable at time t ,

$$c_{\text{pot}}(t) = c_{\text{pot}}^{U_2}(t) + c_{\text{pot}}^{U_1}(t), \quad (27)$$

which determines the tracing efficiency (see equation (9))

$$\varepsilon(t) = \frac{\Omega}{\|(c_{\text{pot}}(t), \Omega)\|_p}. \quad (28)$$

The actual rates at which infected contacts are quarantined at time t are then given by

$$c_{\text{act}}^{\text{inf}, U_1}(t) = c_{\text{pot}}^{\text{inf}, U_1}(t) \varepsilon(t), \quad (29)$$

$$c_{\text{act}, U_1}^{\text{inf}, U_2}(t) = c_{\text{pot}, U_1}^{\text{inf}, U_2}(t) \varepsilon(t), \quad (30)$$

$$c_{\text{act}, U_2}^{\text{inf}, U_2}(t) = c_{\text{pot}, U_2}^{\text{inf}, U_2}(t) \varepsilon(t). \quad (31)$$

In order to approximate from which compartment the infected contacts described by these rates originate, we use the durations (26),(22),(23) and follow the first-order kinetics of system (14). To this end, we solve the initial-value problem

$$\begin{aligned}
\frac{d\tilde{E}}{ds} &= -\alpha\tilde{E} \\
\frac{d\tilde{U}_1}{ds} &= -(\gamma_1 + \eta_{U_1}(t - \kappa))\tilde{U}_1 + \alpha\tilde{E} \\
\frac{d\tilde{U}_2}{ds} &= -(\gamma_2 + \eta_{U_2}(t - \kappa))\tilde{U}_2 + \gamma_1\tilde{U}_1 \\
\tilde{E}(0) &= 1 \\
\tilde{U}_1(0) &= 0 \\
\tilde{U}_2(0) &= 0
\end{aligned}$$

and evaluate the solution at time $s = \tilde{r}^{U_1}(t)$ when considering contacts of U_1 -index cases; at time $s = \tilde{r}_{U_1}^{U_2}(t)$ for contacts of U_2 -index cases that were infected when the respective index case was in U_1 ; and at time $s = \tilde{r}_{U_2}^{U_2}(t)$ when considering contacts of U_2 -index cases that were infected when the respective index case was in U_2 . This results in fractions $\mu_E^{U_1}(t)$ of (29), $\mu_{U_1,E}^{U_2}(t)$ of (30) and $\mu_{U_2,E}^{U_2}(t)$ of (31) originating from the E compartment. Similarly, we get fractions $\mu_{U_1}^{U_1}(t)$ of (29), $\mu_{U_1,U_1}^{U_2}(t)$ of (30) and $\mu_{U_2,U_1}^{U_2}(t)$ of (31) originating from the U_1 compartment and lastly fractions $\mu_{U_2}^{U_1}(t)$ of (29), $\mu_{U_1,U_2}^{U_2}(t)$ of (30) and $\mu_{U_2,U_2}^{U_2}(t)$ of (31) originating from the U_2 compartment.

We end up with the following terms describing contact tracing

$$\begin{aligned}
Tr_E(t) &= \mu_E^{U_1}(t)c_{\text{act}}^{\text{inf},U_1}(t) + \mu_{U_1,E}^{U_2}(t)c_{\text{act},U_1}^{\text{inf},U_2}(t) + \mu_{U_2,E}^{U_2}(t)c_{\text{act},U_2}^{\text{inf},U_2}(t), \\
Tr_{U_1}(t) &= \mu_{U_1}^{U_1}(t)c_{\text{act}}^{\text{inf},U_1}(t) + \mu_{U_1,U_1}^{U_2}(t)c_{\text{act},U_1}^{\text{inf},U_2}(t) + \mu_{U_2,U_1}^{U_2}(t)c_{\text{act},U_2}^{\text{inf},U_2}(t), \\
Tr_{U_2}(t) &= \mu_{U_2}^{U_1}(t)c_{\text{act}}^{\text{inf},U_1}(t) + \mu_{U_1,U_2}^{U_2}(t)c_{\text{act},U_1}^{\text{inf},U_2}(t) + \mu_{U_2,U_2}^{U_2}(t)c_{\text{act},U_2}^{\text{inf},U_2}(t).
\end{aligned}$$

In the setting of this model we get three different tracing coverages for the three different types of secondary infections. The tracing coverage for individuals who got infected by U_1 -index cases is given by

$$\omega^{U_1}(t) := \frac{|J_{t,T}^{U_1,\text{pre}}|}{\tau_t^{U_1}} \frac{\tilde{\beta}_1}{\beta_{U_1}}. \quad (32)$$

The tracing coverage for individuals who got infected by U_2 -index cases when these respective index cases were in U_1 , is given by

$$\omega_{U_1}^{U_2}(t) := \frac{|J_{t,T}^{U_2,\text{pre}}|}{\tau_t^{U_2,U_1}} \frac{\tilde{\beta}_1}{\beta_{U_1}}. \quad (33)$$

Lastly, the tracing coverage for individuals who got infected by U_2 -index cases when these respective index cases were in U_2 , is given by

$$\omega_{U_2}^{U_2}(t) := \frac{|J_{t,T}^{U_2,\text{sym}}|}{\tau_t^{U_2,U_2}} \frac{\tilde{\beta}_2}{\beta_{U_2}}. \quad (34)$$

We could continue with this scheme and divide the infectious period in more and more subperiods. In this way we could approximate a realistic infectivity profile along the infectious period more closely. Alternatively, a more elegant approach is to continuously structure the infected compartment by age of infection [4, 16, 25, 26, 35–37]. However, the ansatz presented here suffices to illustrate the adverse effect of a presymptomatic infectious period on TTIQ effectiveness.

Appendix B Modeling social and hygiene measures and changes in the tracing coverage

In this section we discuss in more detail how changes in social and hygiene measures (that is, non constant transmission rates) and measures affecting the tracing coverage (like changes in the close contact definition or an increasing awareness to keep contact diaries) are modeled in this work. For the sake of simplicity, we explain our approach and assumptions by means of the model with uniform infectious period (4). We proceeded similar for the model with presymptomatic transmissions (14) and briefly comment on this case at the end of this section.

We assume that measures affecting the tracing coverage deviate the contact tracing parameters discontinuously with respect to different "generations" of index cases. Specifically, changes taking place from time t on affect only the contact tracing executed on index case that were detected at time $t - \kappa$ or later, even though these might have overlapping tracing intervals with earlier detected index cases. We indicate this time-dependency of the contact tracing parameters by writing $\tilde{p}_t, \tilde{c}_t, \tilde{\beta}_t$ for the infection probability, the contact rate and the transmission rate observed by contact tracing respectively. We refer to this as the contact tracing scheme applied to contacts being traced at time t . Accordingly, the rate at which contacts become traceable at time t reads (compare with equation (7))

$$c_{\text{pot}}(t) = |J_{t,T}| \tilde{c}_t \eta_U(t - \kappa) U(t - \kappa), \quad (35)$$

and the rate at which infected contacts are quarantined at time t is given by (compare with equation (10))

$$c_{\text{act}}^{\text{inf}}(t) = |J_{t,T}^{\text{inf}}| \tilde{\beta}_t \frac{S(t - \kappa)}{N} \eta_U(t - \kappa) U(t - \kappa) \varepsilon(t). \quad (36)$$

As discussed in Section 2.4 changes in the transmission rates are modeled by a time dependent factor $\phi(t) \in [0, 1]$, so that

$$\beta_U(t) = \phi(t) \overline{\beta_U},$$

where $\overline{\beta_U}$ is the baseline transmission rate of the disease corresponding to a phase without any intervention. When there is a reduction in transmission rate in place at some time point t^* so that $\beta_U(t^*) = \phi(t^*) \overline{\beta_U}$ this potentially also affects $\tilde{\beta}_t, \tilde{p}_t, \tilde{c}_t$ along their relevant time intervals $J_{t,T}$ and $J_{t,T}^{\text{inf}}$, for all t for which $t^* \in J_{t,T}$. To account for this, we let $\overline{\tilde{p}_t}, \overline{\tilde{c}_t}$ denote the infection probability and contact rate observed by contact tracing corresponding to a phase without any intervention in combination with the specific contact tracing scheme applied to contacts traced at time t . We express deviations from these baseline values due to social and hygiene measures by $\tilde{\phi}_{1,t}(s)$ and $\tilde{\phi}_{2,t}(s)$, such that

$$\begin{aligned} \tilde{c}_t(s) &= \tilde{\phi}_{1,t}(s) \overline{\tilde{c}_t}, & s \in J_{t,T}, \\ \tilde{p}_t(s) &= \tilde{\phi}_{2,t}(s) \overline{\tilde{p}_t}, & s \in J_{t,T}^{\text{inf}}, \\ \tilde{\beta}_t(s) &= \tilde{p}_t(s) \tilde{c}_t(s), & s \in J_{t,T}^{\text{inf}}, \end{aligned}$$

whereby given a time $s \in J_{t,T}^{\text{inf}}$ we must have $\tilde{\beta}_t(s) \leq \beta(s)$. The quantities $\tilde{\phi}_{1,t}(s)$ and $\tilde{\phi}_{2,t}(s)$ are influenced by the contact tracing scheme applied at time t indicated by the index t and by the social and hygiene measures that were in place during the time index cases are asked to share contacts from, indicated by the argument s . Their values could be derived from detailed index case and contact tracing data. However, in this work we confine ourselves to the simplified (non-generic) setting where

$$\begin{aligned}\tilde{\phi}_{1,t}(s) &= \phi(s), \quad \forall t \text{ and } \forall s \in J_{t,T}, \\ \tilde{\phi}_{2,t}(s) &= 1, \quad \forall t \text{ and } \forall s \in J_{t,T}^{\text{inf}}.\end{aligned}\tag{37}$$

This resembles that a reduction in general transmission rates by the factor ϕ during the tracing interval $J_{t,T}$ reduces contact rates observed by contact tracing at time t by the same factor, independent of the contact tracing scheme applied at time t . However, the corresponding infection probabilities are assumed to be unaffected by the particular value of ϕ .

Equations (35) and (36) require \tilde{c}_t to be constant on $J_{t,T}$ and \tilde{p}_t to be constant on $J_{t,T}^{\text{inf}}$ (otherwise there would appear integrals over the respective interval in these equations). Being aware that this does not hold for \tilde{c}_t when we consider social and hygiene measures as discussed in this section, we assume that T is reasonably small compared to intervals between parameter changes so that we can approximate $\tilde{c}_t \equiv \tilde{c}_t(t - \kappa)$ over $J_{t,T}$. This leads to

$$\omega(t) = \frac{|J_{t,T}^{\text{inf}}|}{\tau_t} \frac{\tilde{\beta}_t(t - \kappa)}{\beta_U(t - \kappa)}$$

being our proxy for the tracing coverage at time t .

The discussed assumptions extend to the model with presymptomatic transmissions (14). Most importantly, we assume that changes to the tracing scheme equally increase or decrease the different tracing coverages (32)-(34), and that changes in the transmission rates β_{U_2} , $\beta_{U_1} = \theta\beta_{U_2}$ affect contact rates observed by contact tracing by the same factor but do not affect the corresponding infection probabilities observed by contact tracing.

Appendix C Parameterization

Our baseline parameter setting is inspired by the spread of COVID-19 in Germany in late summer and fall of 2020. All scenarios considered in Section 3 in which parameter values deviate from this baseline setting are clearly indicated and explained there.

Parameters describing spreading dynamics and disease characteristics are based on literature dedicated to the original strain of SARS-CoV-2 circulating in 2020. We assume a latent phase of about $1/\alpha = 3.5$ days [8]. This latent phase is followed by a presymptomatic infectious phase of about $1/\gamma_1 = 2$ days [6], which together with the latent period of about 3.5 days gives an incubation period of about 5.5 days [3, 45, 46]. We assume that individuals go through an infectious phase of in total about 9 days and accordingly set $1/\gamma_2 = 7$ [3, 6, 7, 9, 10]. The baseline transmission rate in the symptomatic infectious compartment is chosen as $\overline{\beta_{U_2}} = 0.33$. In addition, we set the scaling factor for the transmission rate of presymptomatic infectious individuals to $\theta = 1.5$. At low prevalence, this leads to approximately 40% [3-6] of transmissions that are produced by undetected infectious individuals to originate from the presymptomatic phase and to a basic reproduction number of $\mathcal{R}_0 = (\theta\overline{\beta_{U_2}})/\gamma_1 + \overline{\beta_{U_2}}/\gamma_2 = 3.3$ [3, 47-49].

For the maximal number of tests that can be administered and evaluated per day²¹ we assume a baseline value of $\sigma_+ = 200\,000$. Notice that we do not consider the additional effort generated

²¹We only consider polymerase chain reaction tests as rapid antigen tests were not yet widely available in 2020.

by testing uninfected traced individuals, the fact that (suspected) cases might be tested repeatedly or the possibility that all individuals might seek more testing at higher prevalence. Therefore, we choose a relatively low value for σ_+ when compared to the theoretical testing capacity reported for Germany in late summer and fall of 2020 [50]. The decay term of tests is set to $\sigma_- = 1.353 N$ such that at low prevalence only approximately 85 000 tests are conducted per day. This roughly aligns with the reports for Germany during summer of 2021 at which time the reported incidence was indeed low [50]²². The relative frequencies (σ_{U_2}, σ_Q) of testing undetected symptomatic and traced individuals compared to susceptibles depend on the considered disease, the testing strategy and the willingness of infected/suspected individuals to get tested. Here we set $(\sigma_{U_2}, \sigma_Q) = (93, 300)$ where we assume $\sigma_Q := \sigma_{Q_E} = \sigma_{Q_{U_1}} = \sigma_{Q_{U_2}}$. Individuals in all the other compartments (importantly also those in U_1) are assumed to not have an increased chance of being tested when compared to a susceptible individual. This results in a detection ratio of about 40% at low prevalence by testing alone. For simplicity, we choose to work with a constant tracing window $T = 1/\gamma_1 + 1/\gamma_2$, which reflects the theoretical decision to trace contacts of an index case for the average duration of the infectious period. We assume that the tracing scheme leads to a baseline value of $\tilde{c} = 0.8$ for the close contact rate reported by an interviewed index case when no contact restrictions are in place. Together with correspondingly selected infection probabilities this results in a tracing coverage of $\omega = 0.65$ (below we discuss why do not have to give different values to the different tracing coverages (32)-(34)). The maximal rate at which contacts can be quarantined per day is assumed to be $\Omega = 40\,000$. Moreover, we assume a tracing delay of $\kappa = 2$ days and a tracing efficiency constant of $p = 2$ (a higher p appears to be unrealistic considering the 400 locally managed public health departments in Germany). The total population size is set to $N = 83\,000\,000$ corresponding to the German population as of 2020.

Our parameter choices are summarized in Table 2 in the main text. While we are aware that parameters change much more dynamically in reality, we keep them constant in the considered simulations, apart from single change points.

Tracing terms resulting from the baseline parameter choices

Here we specify the exact form of the different components included in the contact tracing terms $Tr_E(t)$, $Tr_{U_1}(t)$, $Tr_{U_2}(t)$ in model (14) given our above assumptions on parameter choices and the assumptions made in Appendix B.

We approximate the periods the different types of index cases, as discussed in Appendix A, identified and isolated at time $t - \kappa$ spent in U_1 and U_2 before being detected as

$$\tau_t^{U_1} = \tau_{t, U_1}^{U_2} = \frac{1}{\eta_{U_1}(t - \kappa) + \gamma_1}, \quad \tau_{t, U_2}^{U_2} = \frac{1}{\eta_{U_2}(t - \kappa) + \gamma_2}, \quad (38)$$

which, considering equations (18), (19) and (24), together with the tracing window $T = 1/\gamma_1 + 1/\gamma_2$, leads to the approximations

$$\begin{aligned} |J_{t, T}^{U_1}| &= |J_{t, T}^{U_2}| = \frac{1}{\gamma_1} + \frac{1}{\gamma_2}, \\ |J_{t, T}^{U_1, \text{pre}}| &= |J_{t, T}^{U_2, \text{pre}}| = \frac{1}{\eta_{U_1}(t - \kappa) + \gamma_1}, \\ |J_{t, T}^{U_2, \text{sym}}| &= \frac{1}{\eta_{U_2}(t - \kappa) + \gamma_2}. \end{aligned} \quad (39)$$

²²It should be noticed, however, that the test capacity in 2021 was significantly increased compared to the considered period of late summer and fall of 2020. Nevertheless, our rough approach captures the detrimental effect of an increasing incidence on successful index case identification under limited testing capacities.

Using equations (27), (29)-(31), (26), (22) and (23) we get (respecting the assumptions in Appendix B)

$$\begin{aligned}
c_{\text{pot}}(t) &= \left(\frac{1}{\gamma_1} + \frac{1}{\gamma_2} \right) \tilde{c}_t(t - \kappa) (\eta_{U_1}(t - \kappa)U_1(t - \kappa) + \eta_{U_2}(t - \kappa)U_2(t - \kappa)), \\
c_{\text{act}}^{\text{inf},U_1}(t) &= \frac{\tilde{\beta}_{t,1}(t - \kappa)}{\eta_{U_1}(t - \kappa) + \gamma_1} \frac{S(t - \kappa)}{N} \eta_{U_1}(t - \kappa)U_1(t - \kappa)\varepsilon(t), \\
c_{\text{act},U_1}^{\text{inf},U_2}(t) &= \frac{\tilde{\beta}_{t,1}(t - \kappa)}{\eta_{U_1}(t - \kappa) + \gamma_1} \frac{S(t - \kappa)}{N} \eta_{U_2}(t - \kappa)U_2(t - \kappa)\varepsilon(t), \\
c_{\text{act},U_2}^{\text{inf},U_2}(t) &= \frac{\tilde{\beta}_{t,2}(t - \kappa)}{\eta_{U_2}(t - \kappa) + \gamma_2} \frac{S(t - \kappa)}{N} \eta_{U_2}(t - \kappa)U_2(t - \kappa)\varepsilon(t), \\
\tilde{r}^{U_1}(t) &= \kappa + \frac{1}{2} \frac{1}{\eta_{U_1}(t - \kappa) + \gamma_1}, \\
\tilde{r}_{U_1}^{U_2}(t) &= \kappa + \frac{1}{2} \frac{1}{\eta_{U_1}(t - \kappa) + \gamma_1} + \frac{1}{\eta_{U_2}(t - \kappa) + \gamma_2}, \\
\tilde{r}_{U_2}^{U_2}(t) &= \kappa + \frac{1}{2} \frac{1}{\eta_{U_2}(t - \kappa) + \gamma_2}.
\end{aligned}$$

Considering equations (32)-(34), the approximations (38) and (39), together with assumption (20) and the assumptions in Appendix B, lead to a single tracing coverage

$$\omega(t) := \omega^{U_1}(t) = \omega_{U_1}^{U_2}(t) = \frac{\tilde{\beta}_{t,1}(t - \kappa)}{\beta_{U_1}(t - \kappa)} = \frac{\tilde{\beta}_{t,2}(t - \kappa)}{\beta_{U_2}(t - \kappa)} = \omega_{U_2}^{U_2}(t).$$

Appendix D Stability analysis

The stability of the DFE is approached by considering the linearization about the DFE of system (14) [51]. The linearization of a system of delay differential equations with a single constant delay takes the form

$$x'(t) = Ax(t) - Bx(t - \kappa) \tag{40}$$

with matrices A and B depending on the parameters of the considered system. We consider the linearization of model (14) with respect to the variables²³ $x = (E, Q_E, U_1, Q_{U_1}, I_1, U_2, Q_{U_2}, I_2)$. The corresponding matrices are given by

$$A = \begin{bmatrix}
-\alpha & 0 & \beta_{U_1} & pQ\beta_{U_1} & pI\beta_{U_1} & \beta_{U_2} & pQ\beta_{U_2} & pI\beta_{U_2} \\
0 & -\alpha & 0 & 0 & 0 & 0 & 0 & 0 \\
\alpha & 0 & -(\overline{\eta_{U_1}} + \gamma_1) & 0 & 0 & 0 & 0 & 0 \\
0 & \alpha & 0 & -(\overline{\eta_{Q_{U_1}}} + \gamma_1) & 0 & 0 & 0 & 0 \\
0 & 0 & \overline{\eta_{U_1}} & \overline{\eta_{Q_{U_1}}} & -\gamma_1 & 0 & 0 & 0 \\
0 & 0 & \gamma_1 & 0 & 0 & -(\overline{\eta_{U_2}} + \gamma_2) & 0 & 0 \\
0 & 0 & 0 & \gamma_1 & 0 & 0 & -(\overline{\eta_{Q_{U_2}}} + \gamma_2) & 0 \\
0 & 0 & 0 & 0 & \gamma_1 & \overline{\eta_{U_2}} & \overline{\eta_{Q_{U_2}}} & -\gamma_2
\end{bmatrix},$$

²³The equation for R is encoded in the remaining state variables and the equation for S only gives a zero eigenvalue since all disease free states are equilibrium solutions.

$$B = \begin{bmatrix} 0 & 0 & -\chi_E^{U_1} & 0 & 0 & -\chi_E^{U_2} & 0 & 0 \\ 0 & 0 & \chi_E^{U_1} & 0 & 0 & \chi_E^{U_2} & 0 & 0 \\ 0 & 0 & -\chi_{U_1}^{U_1} & 0 & 0 & -\chi_{U_1}^{U_2} & 0 & 0 \\ 0 & 0 & \chi_{U_1}^{U_1} & 0 & 0 & \chi_{U_1}^{U_2} & 0 & 0 \\ 0 & 0 & 0 & 0 & 0 & 0 & 0 & 0 \\ 0 & 0 & -\chi_{U_2}^{U_1} & 0 & 0 & -\chi_{U_2}^{U_2} & 0 & 0 \\ 0 & 0 & \chi_{U_2}^{U_1} & 0 & 0 & \chi_{U_2}^{U_2} & 0 & 0 \\ 0 & 0 & 0 & 0 & 0 & 0 & 0 & 0 \end{bmatrix},$$

where

$$\begin{aligned} \chi_E^{U_1} &= \left| J_{t,T}^{U_1, \text{pre}} \right|_{\text{DFE}} \tilde{\beta}_1 \overline{\eta_{U_1}} \mu_E^{U_1} \Big|_{\text{DFE}}, \\ \chi_E^{U_2} &= \left| J_{t,T}^{U_2, \text{pre}} \right|_{\text{DFE}} \tilde{\beta}_1 \overline{\eta_{U_2}} \mu_{U_1, E}^{U_2} \Big|_{\text{DFE}} + \left| J_{t,T}^{U_2, \text{sym}} \right|_{\text{DFE}} \tilde{\beta}_2 \overline{\eta_{U_2}} \mu_{U_2, E}^{U_2} \Big|_{\text{DFE}}, \\ \chi_{U_1}^{U_1} &= \left| J_{t,T}^{U_1, \text{pre}} \right|_{\text{DFE}} \tilde{\beta}_1 \overline{\eta_{U_1}} \mu_{U_1}^{U_1} \Big|_{\text{DFE}}, \\ \chi_{U_1}^{U_2} &= \left| J_{t,T}^{U_2, \text{pre}} \right|_{\text{DFE}} \tilde{\beta}_1 \overline{\eta_{U_2}} \mu_{U_1, U_1}^{U_2} \Big|_{\text{DFE}} + \left| J_{t,T}^{U_2, \text{sym}} \right|_{\text{DFE}} \tilde{\beta}_2 \overline{\eta_{U_2}} \mu_{U_2, U_1}^{U_2} \Big|_{\text{DFE}}, \\ \chi_{U_2}^{U_1} &= \left| J_{t,T}^{U_1, \text{pre}} \right|_{\text{DFE}} \tilde{\beta}_1 \overline{\eta_{U_1}} \mu_{U_2}^{U_1} \Big|_{\text{DFE}}, \\ \chi_{U_2}^{U_2} &= \left| J_{t,T}^{U_2, \text{pre}} \right|_{\text{DFE}} \tilde{\beta}_1 \overline{\eta_{U_2}} \mu_{U_1, U_2}^{U_2} \Big|_{\text{DFE}} + \left| J_{t,T}^{U_2, \text{sym}} \right|_{\text{DFE}} \tilde{\beta}_2 \overline{\eta_{U_2}} \mu_{U_2, U_2}^{U_2} \Big|_{\text{DFE}}, \end{aligned}$$

and $\overline{\eta_X}$ denotes the detection rate in compartment X evaluated at the disease-free equilibrium.

The qualitative behavior of solutions of system (40) is determined by the roots of the characteristic equation of (40) given by

$$\det(-\lambda I + A + e^{-\lambda \kappa} B) = 0. \quad (41)$$

In order to numerically approximate solutions of (41) a discretization of the PDE-representation of the DDE can be used. This discretization results in a matrix whose eigenvalues are approximations for solutions of (41). To this end, we followed the discretization scheme based on a Chebyshev nodes described in [52]. The necessary code presented in [52] and [53] was – like all numerical experiments in this work – implemented in Python [54–58]. We calculated the maximum allowed level ϕ^* of effective contacts introduced in Appendix B by scanning for the threshold level in effective contacts which determines a stability switch. In other words, for $\phi < \phi^*$ equation (41) has only solutions with negative real part and the DFE is stable. For $\phi > \phi^*$ there is at least one solution of (41) with positive real part and the DFE is unstable.